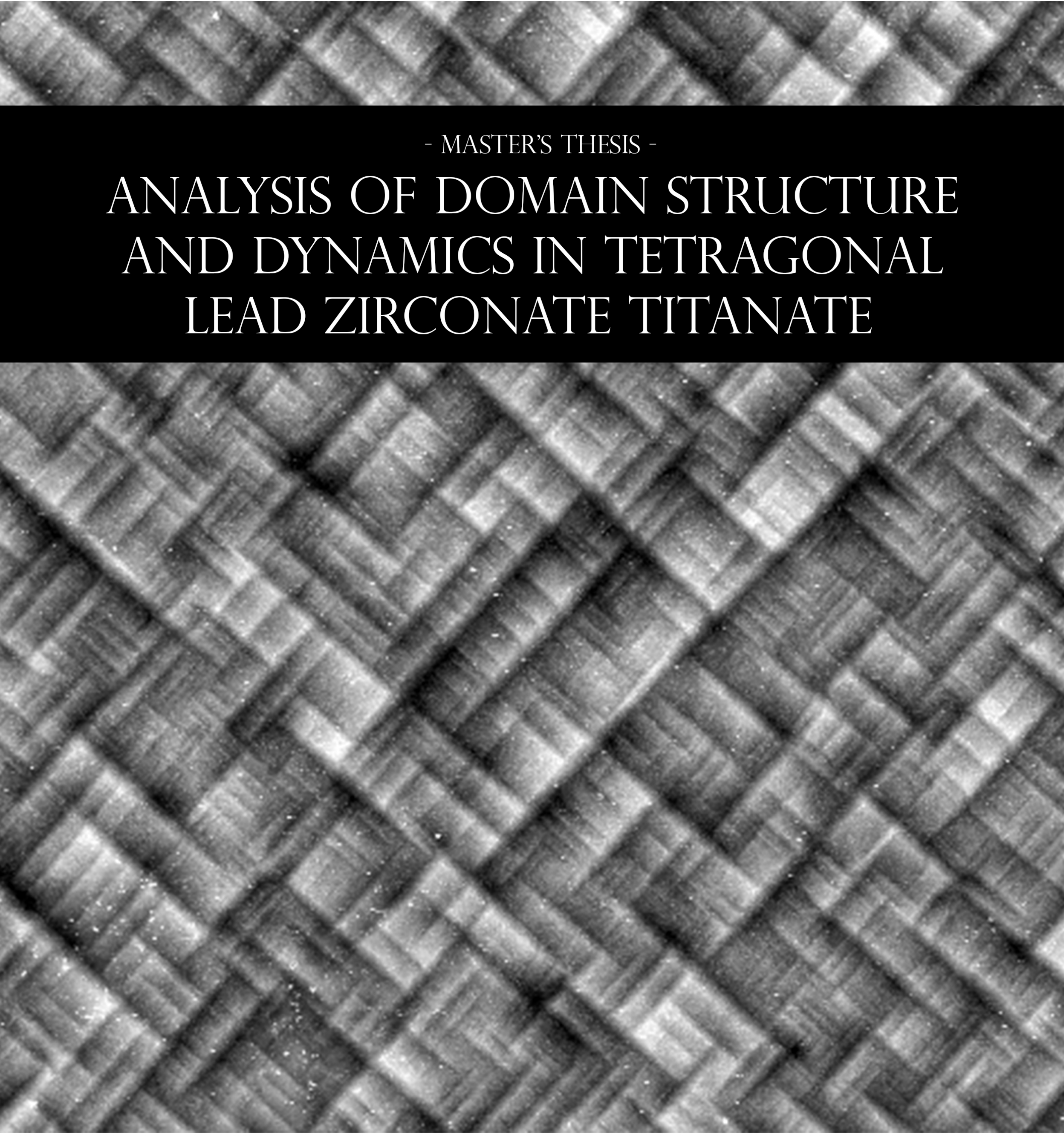

- MASTER'S THESIS -

ANALYSIS OF DOMAIN STRUCTURE AND DYNAMICS IN TETRAGONAL LEAD ZIRCONATE TITANATE

THOMAS A. AUKES
13 MARCH 2015
APPLIED PHYSICS
FACULTY OF SCIENCE AND TECHNOLOGY
INORGANIC MATERIALS SCIENCE GROUP

GRADUATION COMITTEE:
PROF. DR. ING. G. RIJNDERS
PROF. DR. IR. G. KOSTER
PROF. DR. IR. A. BRINKMAN
IR. K. VERGEER

UNIVERSITY OF TWENTE.

MESA+
INSTITUTE FOR NANOTECHNOLOGY

Analysis of domain structure and dynamics in tetragonal Lead Zirconate Titanate

Thomas A. Aukes
Master Applied Physics
Inorganic Materials Science group
Faculty of Science and Technology
University of Twente

March 13, 2015

Abstract

This research is about the domain structure and dynamics in tetragonal compositions of Lead Zirconate Titanate (PZT) epitaxial grown on Strontium Titanium Oxide (STO). PZT and a Strontium Ruthenate Oxide (SRO) bottom-electrode layer were grown on single terminated STO substrates using Pulsed Laser Deposition. To relax the misfit strain imposed by the STO substrate upon cooling down from deposition temperature, the PZT thin film forms a typical tetragonal a/c-domain structure. The PZT film was ferroelectrically switched using a thin metal top-electrode. Before and after switching, the domain structure was studied using different techniques like X-ray Diffraction (XRD), Transmission Electron Microscopy (TEM) and Atomic Force Microscopy (AFM). The TEM indicated the presence of the a/c-domain structure and confirmed the expected relation between the surface height profile and the underlying domain structure. The height profile is used to map the domain structure with an AFM setup. In both XRD and AFM analysis a reconfiguration of the domain structure is observed, thereby indicating movement of the domains. In XRD it is observed that the structural changes relax back to it's as-grown state. A different behavior is observed for different tetragonal compositions of the PZT, which is likely to arise from the difference in tetragonality between both compositions.

Contents

1 Introduction **4**

2 Theory **6**

2.1 Piezo- and ferroelectricity . . . 6

2.2 Tetragonal ferroelectric domains in PZT thin films . . . 7

2.2.1 Tetragonal twinning . . . 10

2.3 Intrinsic and extrinsic piezoelectric effect . . . 11

3 Experimental **13**

3.1 Sample fabrication . . . 13

3.1.1 Pulsed laser deposition . . . 13

3.1.2 Substrate termination . . . 14

3.1.3 Top and bottom electrodes . . . 16

3.2 Characterization methods . . . 17

3.2.1 Atomic Force Microscopy . . . 17

3.2.2 Piezoresponse Force Microscopy . . . 18

3.2.3 X-ray diffraction . . . 19

3.2.4 Transmission electron microscopy . . . 21

3.2.5 Ferroelectric tester . . . 22

3.3 This research . . . 23

3.3.1 Movement of 90°-domains . . . 23

3.3.2 The structure of this research 24
3.3.3 *In-situ* ferroelectric switching in an AFM measurement . . . 24

4 X-ray analysis 26

4.1 Reciprocal space map analysis 26
4.1.1 PZT(37/63) 26
4.1.2 PZT(20/80) 29
4.2 Voltage switching experiments in PZT(20/80) 31
4.3 Discussion 32
4.4 Conclusions 33

5 TEM cross-section analysis 35

5.1 Domain configuration 35
5.2 Domain fraction 38
5.3 Difference in switching and non-switching 40
5.4 Discussion 41
5.5 Conclusions 42

6 Mapping the domain structure 43

6.1 Scanning probe surface analysis 43
6.1.1 Atomic force microscopy 43
6.1.2 Piezoresponse force microscopy 45
6.2 Sub-domain pattern 46
6.3 Discussion 50
6.4 Conclusions 51

7 Mapping the domain dynamics 52

7.1 PZT 37/63 52
7.2 PZT 20/80 56

7.3 discussion 57
7.4 Conclusions 58

8 Conclusions 60

8.1 General conclusions 60
    8.1.1 Mapping the domain dynamics 60
    8.1.2 Thin top-electrode 61
8.2 Discussion and recommandations 61
    8.2.1 Domain fractions 61
    8.2.2 Sub-domain patterns 63
    8.2.3 Top-electrode 63
    8.2.4 Microlines 64
    8.2.5 Domain movement in XRD analysis 65

Chapter 1

Introduction

This thesis is about the dynamics and structure of different tetragonal domains in Lead Zirconate Titanate ($PbZr_{1-x}Ti_xO_3$), also known as PZT. Ferroelectric and piezoelectric materials like PZT are increasingly being considered as critical components in next-generation logic, non-volatile memories, actuators and sensors, and electro-optic elements for waveguide devices. Previous studies have shown that the piezoelectric properties of perovskite ferroelectric films are highly correlated to the dynamics of the ferroelectric domains [1]. Although many has been studied about ferroelectric switching, much remains to be understood about the dynamics of domains during the switching process in complex domain structures and in devices [2].

Recent X-ray diffraction Measurements indicate the movement of ferroelectric domains in a $PbZr_{0.4}Ti_{0.6}O_3$ sample upon switching the material above it's coercive field [3]. The observation of domain movement using the change in intensities in X-ray diffraction reciprocal space map-scans is a relative new way of approaching the problem. The technique undoubtedly indicates a structural change in the materials domain configuration, however because this technique probes relative large areas of the sample it only gives a global indication of what is happening.

To support the conclusions from the X-ray diffraction analysis, it would be interesting to observe the dynamics of tetragonal domains using a more local mapping technique like *Atomic force microscopy* or *Piezoresponse force microscopy.* Using these techniques it is possible to construct a real space image of the height profile or the polarization structure at the surface of a thin film. Since it is expected that the height profile of an epitaxial grown thin film of tetragonal PZT can be translated to the underlying domain structure, it would be interesting to use this technique to observe the structural changes in the domain configuration upon ferroelectric switching. The goal of this research is to investigate the relation between surface height profile and domain configuration, and to use this knowledge to observe and map the the dynamical behavior of tetragonal domains in PZT.

In the first part of this thesis the theory is explained behind the materials that are used. It is explained why the PZT thin film that is used grows in a typical domain structure and why this domain structure is expected to leave a certain roughness pattern at the thin films surface. In the second part, the experimental section, the sample preparation process and the different measurement techniques that are used throughout this research are explained. The next chapters are used to describe the experiments that have been performed in order to achieve the goal of this research. Each chapter presents data on a specific topic and ends with a discussion and conclusion. At the end of the thesis there is a chapter summarizing the conclusions and giving some discussion and recommendations for any possible follow-up research.

Chapter 2

Theory

2.1 Piezo- and ferroelectricity

PZT is a ferroelectric material, which means the material has a built-in spontaneous polarization P_s as a result of the crystal structure. This built-in polarization can be reversed by an externally applied electric field. A material is piezoelectric if a strain is created upon application of an electric field, or an electric field is created as the material is strained. Some of the highest piezoelectric coefficients occur in multicomponent inorganic oxides that have the perovskite unit-cell structure, a few examples are: $BaTiO_3$, $PbZr_{1-x}Ti_xO_3$, $BiFeO_3$ and $LiNbO_3$. In Figure 2.1(a) schematic of the perovskite unit-cell is shown.

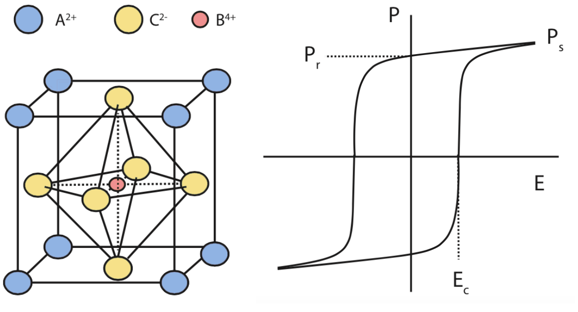

(a) (b)

Figure 2.1: (a) Perovskite unit-cell structure with A, B and C-site ions. (b) typical polarization hysteresis loop [4].

Figure 2.1(b) shows a typical polarization hysteresis loop for ferroelectric materials. Upon increasing or decreasing the externally applied electric field, **E**, the polarization, $\mathbf{P}$, switches at the coercive field $\mathbf{E_c}$. The polarization at zero electric field is called the remnant polarization $\mathbf{P_r}$.

In applications, $PbZr_{1-x}Ti_xO_3$ (PZT) is one of the most used ferro- and piezoelectric materials. PZT is a solid solution of the ferroelectric $PbTiO_3$ and the anti-ferroelectric $PbZrO_3$, with the Lead ions on the A-site of the perovskite structure and a Titanium or Zirconium atom on the B-site (see Figure 2.1(a)). At high temperatures, at which the material is grown, PZT is always in the paraelectric cubic phase. Upon cooling down, the material undergoes a phase change to tetragonal or rhombohedral, depending on the composition. In bulk, PZT is rhombohedral at the Zr-rich side of the phase diagram while it is tetragonal at the Ti-rich side of the phase diagram, as can be seen in Figure 2.2. Throughout this thesis, a composition of $PbZr_{0.2}Ti_{0.8}O_3$ will be named PZT(20/80) meaning 20% Zirconium atoms at B-sites and 80% Titanium atoms.

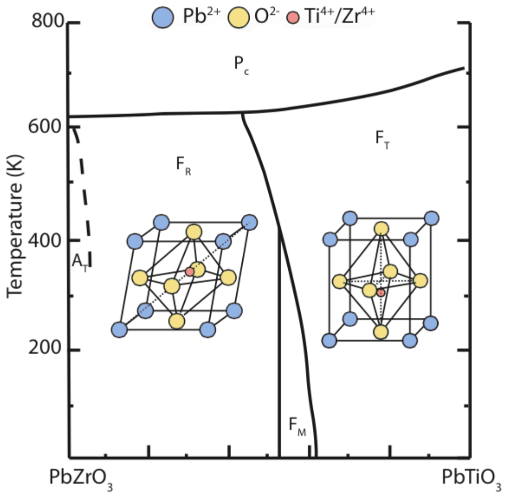

Figure 2.2: Phase diagram for bulk PZT with the ferroelectric rhombohedral phase F_R, the ferroelectric tetragonal phase F_T and the paraelectric cubic phase P_C [4].

2.2 Tetragonal ferroelectric domains in PZT thin films

When a material is epitaxially grown on top of a substrate, a certain epitaxial strain is experienced due to the mismatch between the lattice parameters of the substrate and the thin film. If the unit-cell parameters of both materials are not too far apart, the atoms of the thin film tend to follow the in-plane lattice parameters of the substrate. In this case the out-of-plane lattice parameter is adjusted to conserve the unit-cell volume, this is shown in Figure 2.3(b). This epitaxial strain changes the phase diagram of a material adding an extra strain factor. In Figure 2.3(a) the phase diagram or PZT is shown containing Zirconium content and the extra epitaxial strain.

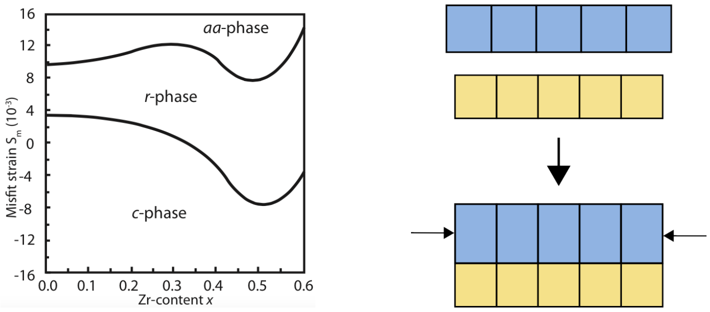

(a) (b)

Figure 2.3: (a) Modeled phase diagram in the case of epitaxial misfit strain [4]. (b) Schematic representation of the epitaxial strain caused by the mismatch in lattice parameters of substrate and thin film.

Usually in films above a certain thickness, >100 nm, the epitaxial stress is relaxed throughout the film by forming dislocations and the lattice parameters become comparable to the bulk values. However, growing PZT thin films on a substrate at high temperatures induces an extra strain on the material due to the difference in thermal expansion coefficients of the thin film and the substrate. Upon cooling down from deposition temperature the thin film mainly follows the shrinkage of the substrate, assuming a much thicker substrate, thereby experiencing either a positive or a negative strain. A way of relaxing the misfit strain in the film is the forming of different polarization domains, this is shown in Figure 2.4(b) by horizontal and vertical standing blocks. In Figure 2.4(a) the modeled phase diagram for the poly-domain PZT films is shown containing the thermally induced misfit strain on the vertical axis. The cubic images picture the different poly-domain phases where the arrows point in the direction of the polarization and the grey area's indicate the orientation of the domain walls.

In Figure 2.4(a) it can be seen that, for most substrates, PZT with low Zirconium content tend to form a tetragonal c/a-phase configuration. This means the film consists of tetragonal unit-cells that form domains in which the unit-cells are oriented with the polarization in-plane (a-domains and b-domains) and out-of-plane (c-domains). Because they are both polarized in-plane, the a- and b-domains are practically the same only one is oriented in the [100] direction and the other in the [010] direction. For tetragonal materials the direction of the polarization is along the longer side of the unit-cell, which implies that unit-cells of the c-domains

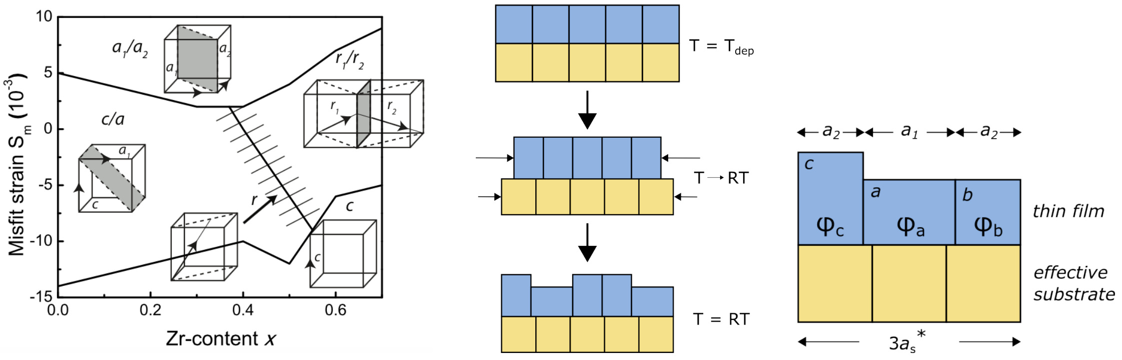

(a) (b) (c)

Figure 2.4: (a) Phase diagram including the thermally induced misfit strain [4]. (b) Schematic representation of the relaxation proces of thermal strain by the formation of different domains. (c) Schematic representation of the relation between the in-plane lattice constants of the thin film and the effective substrate parameter

are longer in the out-of plane direction and of the a- and b-domains are longer in the in-plane direction. These domains are called 90°-domains because the only difference between the two structures is a 90° tilted angle between the polarization vectors.

The theoretical domain fractions for both the out-of-plane c-domains (ϕ_c) and the in-plane a- and b-domains (ϕ_a and ϕ_b) can be calculated from the thermal expansion coefficients and the lattice parameters, this is done using the concept of an effective substrate [13]. Based on the lattice parameters measured at 600°C and room temperature, of both the substrate and the thin film the theoretical value for the domain fraction can be calculated. Below this is done for the case of a PZT thin film grown on an STO substrate. The calculation is done, based on the principle that the amount of b-domains is equal to the amount of a-domains. It is assumed that the STO substrate remains cubic throughout the whole temperature range. The lattice parameters are visualized in Figure 2.5. The effective area's are calculated for the STO substrate and the thin film at 600°C and at room temperature:

$$A_{PZT(600°C)} = d^2_{1(PZT)(600°C)}, \tag{2.1}$$

$$A_{STO(600°C)} = d^2_{1(STO)(600°C)}, \tag{2.2}$$

$$A_{STO(RT)} = d^2_{1(STO)(RT)}, \tag{2.3}$$

$$A_{PZT(RT)} = \phi_c(c_{1(RT)} \cdot c_{2(RT)}) + (1 - \phi_c)(a_{1(RT)} \cdot a_{2(RT)}). \tag{2.4}$$

Upon cooling down the change in area of the STO must be equal to the change in area of the PZT:

$$\frac{A_{STO(600°C)}}{A_{STO(RT)}} = \frac{A_{PZT(600°C)}}{A_{PZT(RT)}} \tag{2.5}$$

$$\frac{d^2_{1(STO)(600°C)}}{d^2_{1(STO)(RT)}} = \frac{d^2_{1(PZT)(600°C)}}{\phi_c(c_{1(RT)} \cdot c_{2(RT)}) + (1-\phi_c)(a_{1(RT)} \cdot a_{2(RT)})} \tag{2.6}$$

Which can be solved to find the c-domain fraction (ϕ_c):

$$\phi_c = \frac{\left(\frac{d^2_{1(PZT)(600°C)} \cdot d^2_{1(STO)(RT)}}{d^2_{1(STO)(600°C)}}\right) - (a_{1(RT)} \cdot a_{2(RT)})}{(c_{1(RT)} \cdot c_{2(RT)}) - (a_{1(RT)} \cdot a_{2(RT)})} \tag{2.7}$$

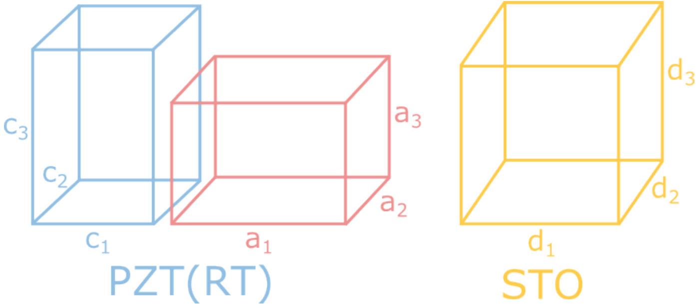

Figure 2.5: Schematic picture of the lattice constants for the tetragonal a-domains (blue), c-domains (red) and the cubic STO (yellow).

2.2.1 Tetragonal twinning

As discussed in the previous section, for certain compositions and strain values the PZT thin film consists of tetragonal a- and c-domains. In order to connect both tetragonal polarization domains on a unit-cell scale, an effect occurs that is called tetragonal twinning. Because both domains must be matched on an atomic level, a tilt angle between both domains is inevitable. This is schematically shown in Figure 2.6. The white areas in Figure 2.6 indicate the domain wall that exists between two different domains and which is oriented roughly 45° with respect to the substrate. Note that the thickness of this domain wall does not necessary has to be one unit-cell.

The tilt angle between the two domains has been studied in work done by Kittel [12]. He calculated the maximum angle between the a- and c-domains, $\Delta\omega_{max}$, as a function of the unit-cell size parameters a_1 and a_3;

$$\Delta\omega_{max} = 2arctan(a_3/a_1) - \pi/2. \tag{2.8}$$

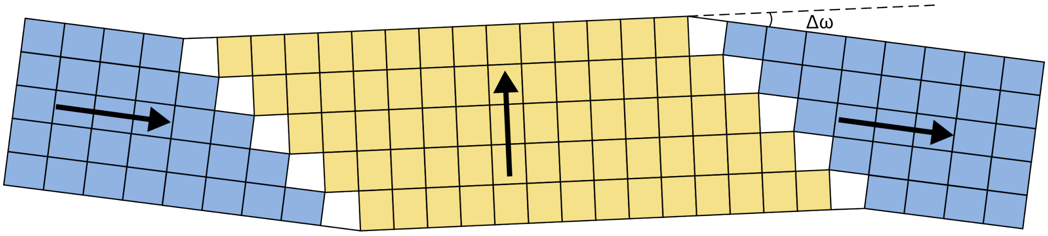

Figure 2.6: Schematic image of the connection of two 90° domains on a unit-cell scale. The arrows indicate the direction of the polarization in the domains, the angle between both domains is indicated in image with $\Delta\omega$.

This maximum angle does not necessarily have to be the actual angle between two domains in a thin film, it just gives a value based on the fact that the unit-cells nee to match on an atomic scale and are fully relaxt as in bulk [11]. Figure 2.6 shows how the tilt angle between the domains causes a surface roughness profile. If a c-domain is tilted towards the left, the connected a-domains must be tilted towards the right. This surface pattern could be measured using an Atomic Force Microscope, and can then be translated back to the underlying domain pattern.

Also the domain fraction can be calculated from the angling of the a- and c-domains, this is done in an article by *Foster et al.* [5] based on coherency strain. One can simply state that for low angles, the angle of the a-domains times the relative amount of a-domains must me equal to the same but then for c-domains, this results in the following formula;

$$\phi_c \omega_c = \omega_a (1 - \phi_c). \tag{2.9}$$

Which can be rewritten to get ;

$$\phi_c = \frac{\omega_a}{\omega_c + \omega_a}. \tag{2.10}$$

2.3 Intrinsic and extrinsic piezoelectric effect

In the field of PZT as a piezoelectric material, it is well known that several factors contribute to the relative high piezoelectric coefficient. This has to do with the fact that the material can grow in different domain structures, as explained in section 2.2.

As explained in section 2.1 a material is piezoelectric when a strain is created upon application of an electric field, or vice versa. In the intrinsic piezoelectric effect this strain arises from a unit-cell distortion, based on the fact that the electric field pushes the ions apart. This can be studied by making single domain films and studying the piezoelectric behavior of this [6, 7]. The intrinsic piezoelectric effect is something that is always present in a ferroelectric material.

The extrinsic piezoelectric contribution is driven by the ferroelastic domain movement of the in section 2.2.1 described domains. Upon applying a voltage across a tetragonal PZT thin film consisting out of a- and c-domains, a fraction of the in-plane oriented a- and b-domains will turn into out-of-plane oriented c-domains. This causes a net strain in the out-of-plane direction. Different articles, for bulk and thin film PZT, claim this effect to be of the order as the intrinsic piezoelectric effect in tetragonal grown PZT thin films [1, 8].

Chapter 3

Experimental

3.1 Sample fabrication

3.1.1 Pulsed laser deposition

In order to grow epitaxial thin films of PZT, a deposition technique is used called Pulsed Laser Deposition (PLD). In this technique a target material is evaporated by locally heating it up by a short and intense laser pulse. Most commonly this is done by excimer lasers (ArF, KrF, XeCl) at repetition frequencies of 1-100 Hz. In order to get the desired energy density, the pulsed and highly energetic laser beam is focussed by a lens on the target material. The vaporized material forms a plume and by placing a substrate inside the plume area some of the material will form a thin film on the substrate.

In the target material, the laser energy is transferred through photon absorption by the electrons of the atomic system. The absorbed energy causes electrons to be in high energetic excited states. As a result, the material heats up to very high temperatures in very short time. Due to this high temperature, material will be evaporated from the surface. The evaporated material will form an expanding gas, which can only expand perpendicular to the surface of the target. Because of relaxation of the excited electrons, the particles will emit light and form a highlighted plume.

The processes inside the plume during transport are highly influenced by the presence of a background gas. By varying the mass and pressure of the gas, the kinetic energy of the particles arriving at the substrate can be tuned. This kinetic energy can be varied from high energy (∼100 eV) in vacuum to low energy (∼1 eV) at large ambient pressures. Because the chemical interactions between the evaporated material and the background gas is critical for the stoichiometrics of the film, the right type of background gas and pressure is of great importance in growing thin films by PLD. All oxide materials consist of positive charged ions, neutralized by negatively charged oxide-ions. Upon vaporizing, the bonds between the oxygen and and the positive ions are almost all gone. (checken?) Vaporizing the material in a oxygen rich environment causes the positive ions in the plume to react with the ambient oxygen before landing on the substrate.

One of the advantages of using PLD for depositing solid solution thin films is the capability for stoichiometric transfer of material from the target to the substrate. This and the ability to use an oxygen background pressure makes the technique ideal for growing thin film oxide materials.

Pulsed laser deposition setup

All samples used in this theses were fabricated using a PLD setup in the MESA+ institute at the University of Twente. A KrF laser with a wavelength of 248 nm is uses with a typical pulse duration of 20-30 ns. The laser beam is shaped using a rectangular shaped mask and is focused on the target material using an optical setup. Prior to deposition the target material is grinded, using sandpaper, and pre-ablated for 2 minutes at 4 Hz. Substrates are attached to a heater using silver-glue for good heat conductance, and are placed inside a vacuum chamber. The laser fluency (intensity) at the target is 2.5 J/cm^2 and a spot size of 2.7 mm^2 is used. Using these parameters a deposition rate of 1 μm/hour is achieved at 10 Hz. In table 3.1, the material specific parameters are listed.

Material	Thickness (nm)	pO_2 (mbar)	T (°C)	Freq. (Hz)	Time (min)
SRO	100	0.13	600	4	20
PZT	1000	0.1	600	10	50

Table 3.1: Used deposition parameters for *Pulsed Laser Deposition.*

3.1.2 Substrate termination

In this research only Strontium Titanium Oxide, $SrTiO_3$ (STO), is used as a substrate to grow the PZT. STO is a non-conducting perovskite and is ideal to grow the SRO and PZT perovskite structures. Because STO has more or less the same lattice parameter as the SRO and PZT that are grown on top, both materials are able to grow in an epitaxial stack. The samples that are used are 5×5 mm^2 and are single side polished by *Crystech*.

One way of looking at the STO crystal is considering it is build up of separate layers of Strontium-oxide and Titanium-oxide. Because the 001-plane of the material always has a certain miscut, step-edges between the Titanium-oxide layers and Strontium-oxide layers are formed at the surface. In most other research on growing thin films on STO, the STO substrates are always single terminated with layers of Titanium-oxide. To be able to compare the observations, this is also done with the samples used in this research. However it needs to be mentioned that for thick layers of PZT, this is not mandatory. To make the Strontium-oxide terminated STO substrates, a typical termination proces is done;

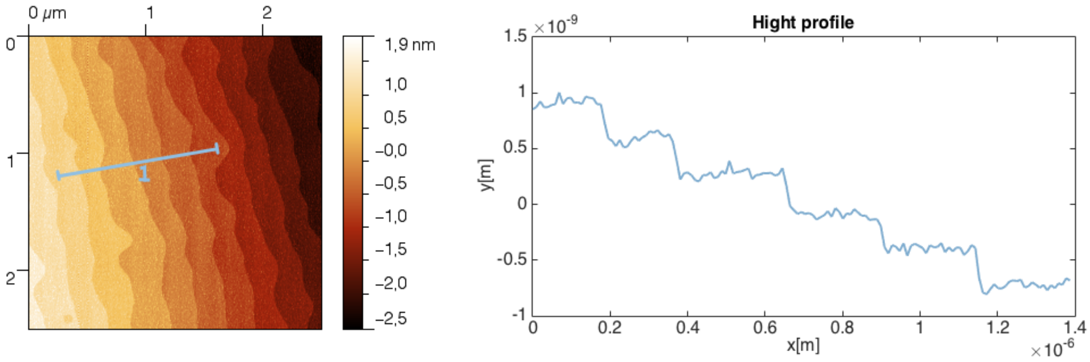

(a) (b)

Figure 3.1: (a) STO topography image made with an Atomic Force Microscope. (b) height profile at the line drawn in (a).

1. The substrate is cleaned, first in Acetone than in Ethanol
2. The substrate is put in the ultrasound bath for 30 seconds in a hydrofluoric acid solution
3. The substrate is put in two different cups with demineralized water, each for 10 seconds
4. The substrate is put in another cup with demineralized water for 30 seconds
5. The substrate is put in the ultrasound bath for 30 seconds in an ethanol solution
6. The substrate is put in an oven at 950 °C for 90 minutes.

Figure 3.1(a) shows the surface topography after the termination process. The step-edges are visible and are all parallel to each other. A height profile is made at the line drawn in Figure 3.1(a) to clarify the step-edge height of about 0.4 nm, the profile is plotted in 3.1(b).

3.1.3 Top and bottom electrodes

In order to apply an electric potential to the PZT top and bottom electrodes are needed. On top of the STO substrate, a SRO layer is grown to function as bottom electrode. SRO is conductive and has the same perovskite unit-cell structure as the PZT. Because the bulk unit-cell size of the SRO is somewhere between that of the STO and the PZT, it also enhances the epitaxial growth of the PZT on top of the STO.

To be able to switch parts of the PZT layer, a top-electrode on top of the PZT thin film is needed. To make a top-electrode, a very thin layer of platina, 8 nm, is grown on top of the sample by a proces that is called microwave sputtering which is done inside the cleanroom facility of MESA+. In this process the material is heated by microwave radiation which causes it to evaporate onto the desired sample. To enhance the sticking of the metal to the PZT surface, a 2 nm titanium adhesion layer is deposited between the platina and the PZT. Titanium can function as adhesion layer between PZT and a metal, like platina, because there is already titanium present in the PZT structure. In an early stage of this research gold was used as top-electrode, it was sputtered the same way as the platina that is mentioned above.

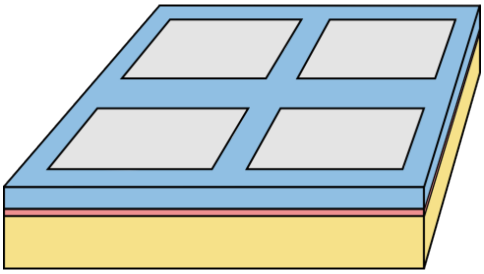

Figure 3.2: Schematic drawing of the sample. The STO substrate is yellow, the SRO is red, the PZT is blue and the platina top-electrodes are grey.

The use of a 5×5 mm^2 sample makes it possible to fit more than one top-electrode on top of the sample. By making four different electrodes, the amount of measurements that can be performed on one sample is higher. The structuring of these top-electrodes is done by a process called lift-off. In lift-off techniques the substrate is first covered in a photoresist layer which is patterned by a photolithography process. The result is a structure where the places that don't need to be covered with platina, or any other material, are covered in a layer of photoresist. After this, the platina is grown on top of the substrate as described above. After growing the top-electrode, the photoresist layer is removed by ultrasonic cleaning in acetone, and the remaining structure consists of the desired pattern.

3.2 Characterization methods

3.2.1 Atomic Force Microscopy

Atomic Force Microscopy (AFM) is a scanning probe type of microscope in which the surface of a substrate is scanned by an atomically sharp tip. The tip is mounted on a cantilever and reacts on the atomic forces that act between tip and substrate surface. To map the three-dimensional surface topography, the tip is raster scanned in x and y over the surface of the sample. A typical AFM setup consists of five basic components; a cantilever with tip, a laser, a four quadrant photodetector, a XYZ-piezoscanner and a feedback control mechanism.

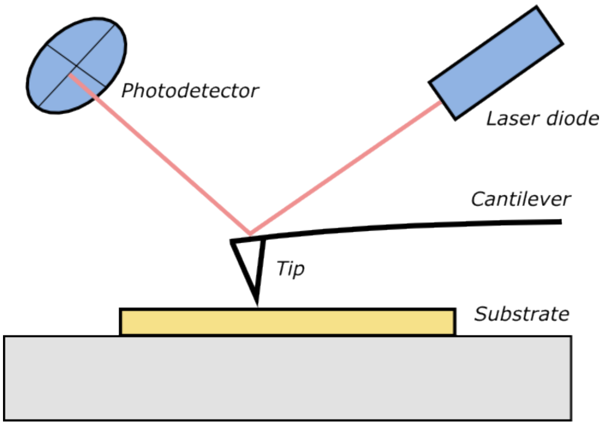

Figure 3.3: Schematic image of AFM setup with laser, photodiode, cantilever and tip (not to scale).

The laser is pointed towards the cantilever and reflects from the back of the cantilever towards the photodetector. Any deviation in the height of the cantilever can be measured as an offset of the laser at the photodiode, this offset is compensated by the electronic feedback mechanism by adjusting the height of the cantilever. This way a surface profile can be constructed of the sample.

There are several ways of operating an AFM but the one used in this research is *Amplitude modulated AFM* (AM-AFM) also referred to as tapping mode. In tapping mode the cantilever is driven into oscillation at a fixed frequency near it's free resonance frequency. Due to tip-sample forces, F_{ts}, the resonance frequency f_0 will shift, which changes the amplitude at the drive frequency. This deflection signal is fed in the feedback loop to keep the oscillation amplitude and therefore the average force constant [9]. The minimum detectable force gradient in AM-AFM is given by;

$$\delta F_{min} \approx \sqrt{\frac{2kBk_BT}{f_0QA^2}} \tag{3.1}$$

In this expression k is the cantilever spring constant, k_BT is the thermal energy, B is the measurement bandwidth, Q is the quality factor of the cantilever, f_0 the resonance frequency and A the mean amplitude. The minimum detectable force depends on the cantilever properties (k, f_0, A, Q), bandwidth (B), temperature (k_BT) and measurement environment (Q). In this research Antimony (n) doped silicon cantilevers are used with a resonance frequency of 320 kHz and a spring constant of 42 N/m.

3.2.2 Piezoresponse Force Microscopy

Piezoresponse Force Microscopy (PFM) is a scanning microscope type of measurement in which the ferroelectric and piezoelectric properties of a material are probed. The technique is especially useful for locally probing ferroelectric domain structures, but can also be very sensitive to disturbances because of the contact mode nature of the technique.

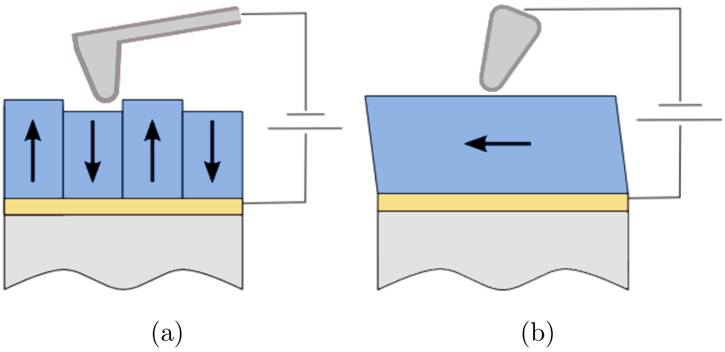
(a) (b)

Figure 3.4: (a) sideview of a cantilever response on a out-of-plane polarized domain structure (b) frontview of a cantilever response on an in-plane polarized domain. [10].

PFM is based on contact mode scanning probe microscopy and is schematically shown in Figure 3.4. The tip used in PFM is coated with a conductive material and functions as a local mobile top-electrode to apply a bias between the tip and sample stage. When an electric field is placed across a piezoelectric material a deformation will occur in the material, this deformation is measured as a deformation in height of the PFM tip. The piezoelectric deformation of the material corresponds to the direction of the ferroelectric polarization, and therefore the domain structure can be probed.

Besides the height profile, the PFM measures two different type of signals, phase and amplitude. The phase signal tells something about the direction of the polarization while the amplitude gives a value for the strength of the polarization. In Figure 3.4(a) the vertical displacement of the sample and tip is schematically shown. Figure 6.3 shows the reaction of the cantilever on a in-plane piezoresponse, which results in a torsion of the cantilever instead of a vertical displacement. It is only possible to measure in-plane polarization that is perpendicular to the cantilever orientation. Piezoresponse along the cantilever direction will not be able to cause a torsion of the tip. The out-of-plane phase and amplitude is measured by the vertical displacement of the cantilever. This signal must be analyzed very carefully because also an in-plane polarization in the direction of the cantilever can cause a vertical displacement signal, this is called buckling of the cantilever.

3.2.3 X-ray diffraction

To investigate the crystal structure of a material, X-ray diffraction (XRD) is a very useful technique. Based on constructive interference of x-ray waves, scattered by unit-cell lattice planes, conclusions can be made about the crystallographic orientations and sizes of a crystal structure.

A coherent X-ray source bombards the sample with a focused monochromatic beam of X-rays. Because the waves will be diffracted by different lattice points inside the crystal, the waves will be scattered in different directions each corresponding to a different lattice plane orientation. By measuring the diffracted waves with a detector, the lattice dimensions can be calculated based on the angles of incident and diffracted waves. The diffracted beams form a pattern that represents the measured crystal in reciprocal space, each point in reciprocal space corresponds to a collection of lattice planes in real space from which the beams are coherently scattered. The angle for which coherent scattering takes place is given by Bragg's law;

$$n\lambda = 2dsin(\theta) \tag{3.2}$$

In the equation, λ is the wavelength of the monochromatic X-ray source (1.54 nm), d is the lattice spacing, n is the order of diffraction and θ is the angle at which the beam is detected. In Figure 3.5 Bragg's law of diffraction is pictured schematically.

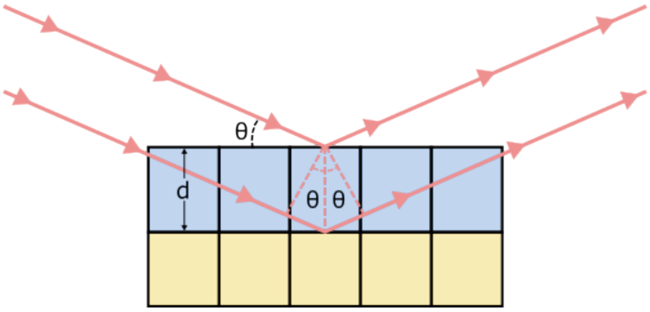

Figure 3.5: Schematic illustration of Bragg's law of diffraction.

The XRD has many different types of measurements, of which a few are used throughout this research. To measure the diffracted beam pattern, a fixed source is pointed at the sample which is oriented under a certain angle (ω) and the detector is moved at certain angles (θ). One type of scan dat is used in this research is an ω-*scan* in which the detector is fixed and only the sample is rotated at certain values. This is clarified in Figure 3.6 by the line indicated by ω. A variant to this scan is the $\omega - \chi$ scan where the sample is tilted in the ω-direction and the χ-direction, which is the direction into the page. Another type of scan that is used is a so called *reciprocal space map*, in this type of scan the detector is rotated certain angles at a range of ω-values, this way a part of reciprocal space can be mapped. This scan is also illustrated in Figure 3.6 by the area that is covered in blue.

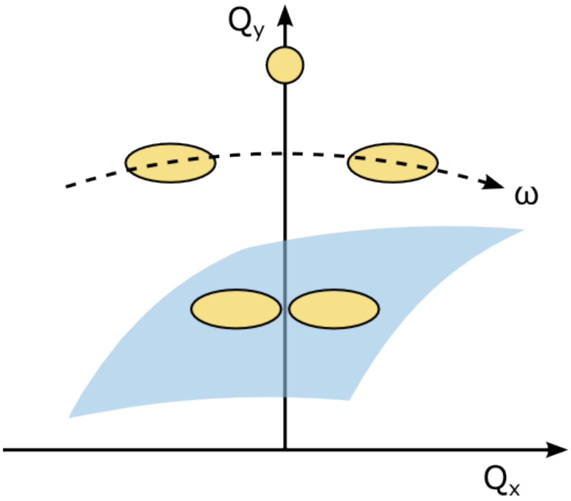

Figure 3.6: Illustration of two different scan types in reciprocal space. The yellow dots represent different diffraction spots from the crystallographic sample, the dashed line represents the direction of a typical ω-scan and the blue area is a typical reciprocal space map scan area.

3.2.4 Transmission electron microscopy

Transmission electron microscopy (TEM) is a technique in which a beam of electrons is transmitted through a thin slice of material and interacts with the crystal lattice. On a fluorescent screen at the back of the sample the electrons form either a diffraction pattern or, by placing a lens, a real time image of the sample. Because electrons exhibit a small de Broglie wavelength, compared to photons, TEM is capable of reaching a higher resolution than optical microscopes that even extends into atomic resolution for certain conditions. Different operating modes are available for the TEM but the one used in this research is *high-resolution transmission electron microscopy* (HR-TEM). In order to make a cross section TEM picture of a sample, the right preparation process is crucial. In this case the sample is first cut into two parts, which are glued face-to-face to each other using a certain kind of wax. A dummy is glued to the to and bottom of the new sample. Then a cylinder is cut out of the sample using an ultrasonic disc cutter. Next, the cylinder needs to be thinned in order to be electron transparent, this can be either mechanically or using ion-beam milling. The sample is then put into the TEM to see if it is thin enough, if not, the sample is thinned a bit more. This proces is repeated until the sample is transparent enough for electrons to do the measurement.

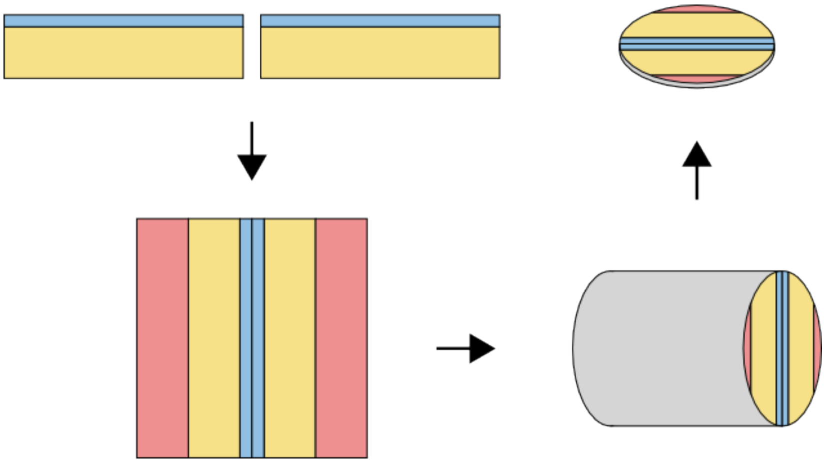

Figure 3.7: Schematic illustration of the cross-section TEM preparation process. In the figure the blue parts are the thin films, the yellow parts are the substrate and the red parts are dummy pieces.

3.2.5 Ferroelectric tester

In order to test the ferroelectric behavior of a grown film, a polarization hysteresis loop is measured like in Figure 2.1(b) using a ferroelectric tester. The polarization hysteresis loop is a direct indication for the quality of the film. Also the voltage that is needed to switch the material, the coercive field, is an important parameter measured by the ferroelectric tester.

To construct the polarization hysteresis loop, also called PE-loop, the ferroelectric tester had several different measurement types. The ones used for this research are *Dynamical Hysteresis Loop*(DHM) and *Pund Measurement*. In DHM mode saw tooth shaped dynamic voltage is applied across the sample at high frequencies, see Figure 3.8(a). Because of the high frequency, the ions don't have the time to move and thereby the contribution of a leakage current is very small. However the high frequency also tends to change the polarization values in the PE-loop, for this reason it is better to do a *pund measurement*. A pund measurement is a pulsed type of measurement where the applied voltage is kept at a certain value for longer, see Figure 3.8(b). This way there is time for a current to flow, in case the sample has a leakage current. The PE-loop that is constructed in this measurement is better for a quantitative analysis of the quality of the sample.

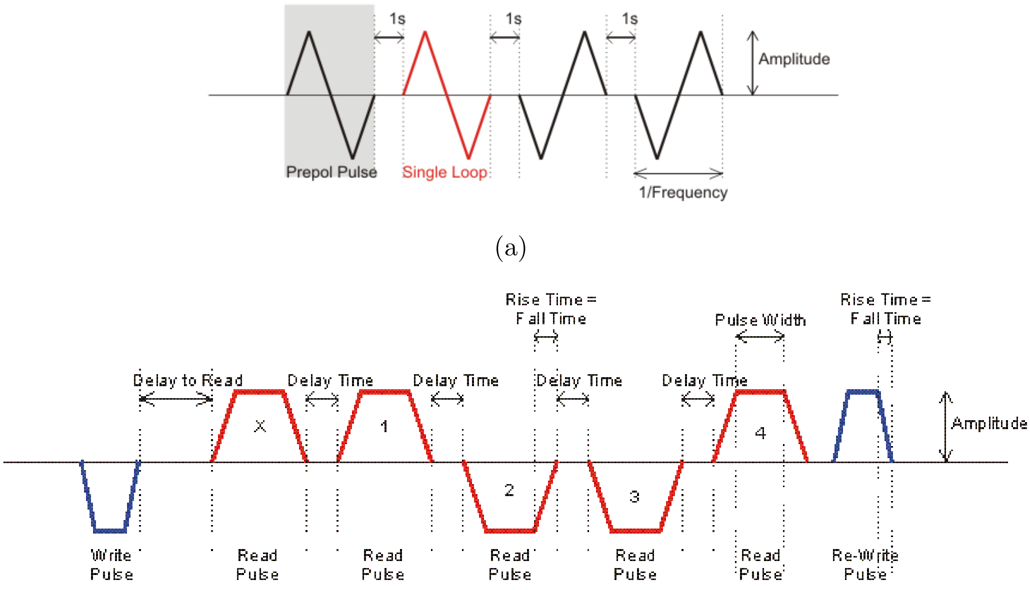

(a)

(b)

Figure 3.8: schematics of the two types of ferroelectric measurements that are used for this research. (a) Dynamical hysteresis loop and (b) pund measurement.

3.3 This research

3.3.1 Movement of 90°-domains

Experimental observations within the IMS group led to the presumption that after ferroelectric switching of the PZT, some of the domains have changed their location. This is a somehow controversial subject within the study of ferroelectrics because both movement and pinning of the domain walls have been observed and reported in the past. Some articles claim that the ability for domain walls to move, and thereby change the domain configuration, contributes to the high piezoelectric coefficients measured in those samples [14–17]. Another article calculated the energy associated with pinning of the domain walls to defects at the film-substrate interface, and claimed that moving of the domain wall was energetically unfavorable [19]. It is not unusual within the field of ferroelectric thin films that each case is different, since many factors play an important role in the behavior of the material.

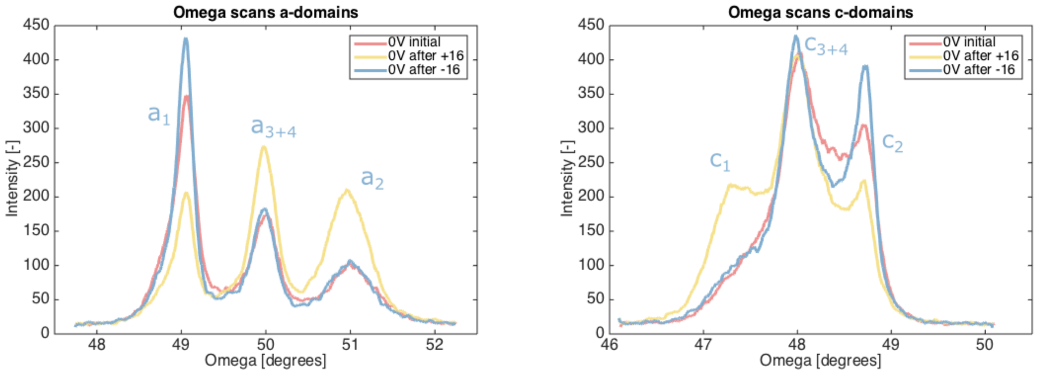

(a) (b)

Figure 3.9: Omega scans of a PZT(40/60) sample at the a-domains (a) and c-domains (b) for three different situations; initial, 0 Volt after switching at +16 Volt and 0 Volt after switching at -16 Volt. The names of the different peaks are given in the graph.

Figure 3.9 shows XRD omega-scans of the a- and c-domains of a PZT(40/60) sample, before and after it was ferroelectrically switched at +16 Volt and -16 Volt [3]. Both graphs show more or less three different peak positions. The two on the side correspond to the left and right tilted domains and the one in the middle comes from diffractions from the domains that are tilted to the front and back (relative from the image plane). When a (positive) voltage is applied to a thin film of a/c-oriented PZT, some of the a-domains become c-domains and the overall thickness of the film increases. This is called the extrinsic piezoelectric effect. When the voltage is removed, the c-domains change back to a-domains and the thickness decreases again. However, the graphs of Figure 3.9 show that some of the domains that were tilted to one side changed their orientation towards the other side, meaning that the configuration of domains in the film is different after it was ferroelectrically switched. The configuration can only be different if the domain-walls moved to some extend, how this happened cannot be derived from the XRD data.

The goal of this research is to see if the above described configurational changes can also be observed with an Atomic Force Microscope. If the domains and thereby the domain-walls change their configuration, because of the tilt angle of the domains a change in the topography of the material should also be observed, see section 2.2.1. The real-space AFM data could give a more local understanding of the phenomena that could complement the more large scale averaged XRD data. These observations could give new insight in the way this domain motion takes place and might give insight in the mechanisms behind it.

3.3.2 The structure of this research

To approach the goal described in section 3.3.1, several steps and experiments are performed. The different chapters in this thesis describe the different experimental steps that have been done. Each chapter discribes the experimental results and is finished with a discussional and concessional section.

1. X-ray analysis is performed to choose the right PZT compositions, and confirm the dynamical domain behavior of these compositions.
2. Then a TEM analysis is done to test if the theoretical predictions from section 2.2.1 about the height profile are correct.
3. AFM and PFM are used to map and study the domain structure at the thin film's surface.
4. Finally an *in-situ* AFM setup is used to observe the dynamical behavior of the PZT thin films.

3.3.3 *In-situ* ferroelectric switching in an AFM measurement

To investigate the dynamical behavior of the ferroelectric domains, AFM measurements where done before and after a voltage was applied across the ferroelectric thin film in order to switch the polarization states. To switch the PZT film and still be able to observe the surface roughness pattern at the film interface, a very thin top-electrode is crucial. As described in section 3.1.3, 8 nm gold or titanium is sputtered on top of the PZT thin film with a 2 nm titanium adhesion layer.

In order to compare the surface pattern before and after switching the PZT film, a measurement setup was needed that allowed a variable voltage to be applied without moving the sample. This way, the AFM tip could be withdrawn from the sample, the PZT could be ferroelectrically switched and the AFM could afterwards approach the sample at the same location as before.

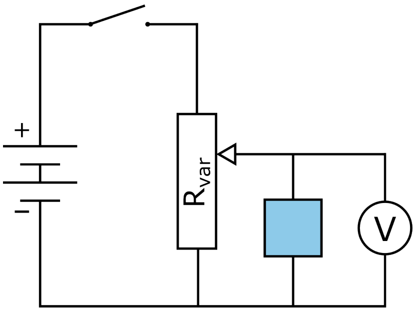

Figure 3.10: Schematics of the electrical circuit that was made to achieve *in-situ* polarization switching.

Figure 3.10 shows the electrical circuit that was made to achieve the *in-situ* switching. The blue square in Figure 3.10 is the sample. The power source consists out of eight 1.5 Volt batteries, connected in series to create a 12 Volt power supply. The variable resistance (R_{var}) is a 5k Ohm potmeter that can vary between 0 and 5000 Ohm. The circuit allows the voltage across the film to be regulated between 0 and 12 Volt.

To contact the electrodes of the sample to the power source the sample was glued on a sample holder that has a copper structure on it. The sample is glued using a current conducting silver glue, which is also put to one side of the sample to contact the back electrode. The top-electrode is contacted using a wire bond from the electrode to another copper line on the sample holder. From the holder, two normal wires form the connection between the plate and the measurement setup.

Chapter 4

X-ray analysis

The goal of this section is to select the different PZT compositions that are used throughout this research. Experimental results from XRD studies are shown, comparing a PZT(37/63) and a PZT(20/80) sample. Also the change in location of the XRD peaks is studied to some extend.

4.1 Reciprocal space map analysis

4.1.1 PZT(37/63)

Prior to this research, XRD experiments were performed on PZT(40/60) samples showing an interesting phenomena, see section 3.3.1. In these experiments, reciprocal map scans were made of a sample before and after it was switched (> 100 cycles) above its coercive field. Because in this research PZT(37/63) is used instead of PZT(40/60), the experiments have been repeated for a PZT(37/63) sample where the same behavior was observed. The map scans of these measurements are shown in Figure 4.1.

In the map scans the substrate peak and peaks for the the different a- and c-domains are shown. The top and most intense peak is the diffraction spot from the STO substrate, below that is the thin film peak for the epitaxial grown SRO bottom electrode. The peaks below that all correspond to the different PZT(37/63) a- and c-domains, it can be seen that both type of domains are tilted to the left and right with respect to the STO out-of-plane crystal axis. The PZT(37/63) peaks in the middle correspond to the domains that are tilted to the front and the back, which can be seen in the scan because of the spread of the measurement beam in

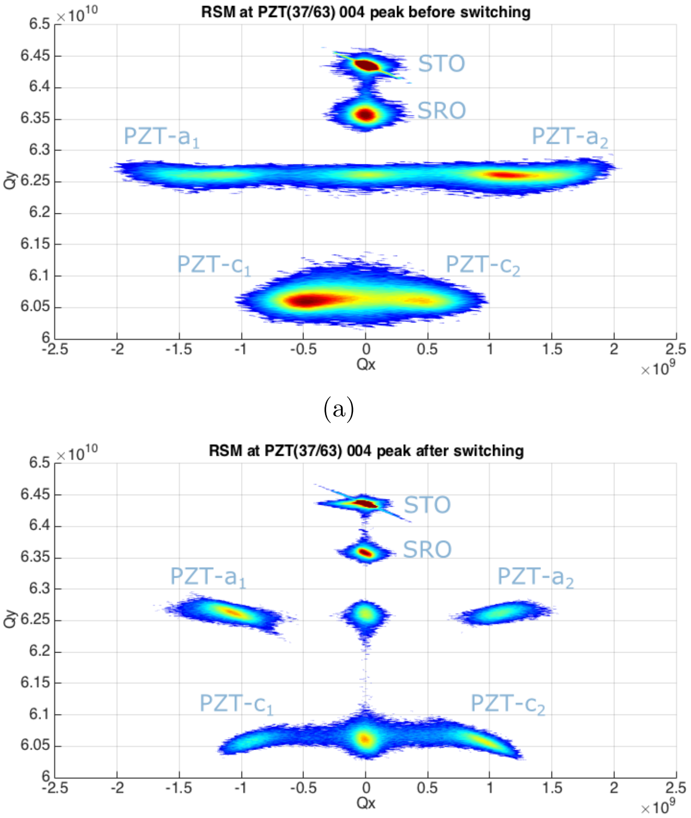

(a)

(b)

Figure 4.1: Reciprocal space maps around the PZT(37/63) 004 peaks. (a) initial and (b) after switching the sample a number of times above the coercive field. The locations for the STO, SRO and different PZT peaks are indicated by the labels in the graphs.

χ-direction.

It is observed that after switching the material above the coercive field, the peaks have changed position. The bottom peaks, originating from the c-domains, both have moved a significant amount to the side. This indicates that the tilting of these domains has increased. Table 4.1 gives the lattice parameters and tilt angles that have been calculated based on the data from Figure 4.1. It can be seen that the tilting angle of the c-domains has almost doubled in value. For the a-domains, after switching the peaks seem to be more localized, showing less spread in the omega direction. The tilt angle for the a-domains slightly decreased, but this is almost nothing compared to the change in the c-domains. It can also be seen in Table 4.1 that the out-of-plane lattice parameters for both domains has slightly increased, this might be accounted to uncertainties in the measurement method. Another observation is that the most intense peak flipped side in both domains, this can however be because one of the two scans was made at a 180° angle with respect to the other. It must be noted that an intens a-domain peak which is tilted to the right, always comes with an intense c-domain peak that is tilted to the left. This makes sense taking Figure 2.6 in account.

	$a_{(001)}$ (Å)	$c_{(001)}$ (Å)	ω_a (deg.)	ω_c (deg.)	$\Delta\omega = \omega_a + \omega_c$
Before switching	4.0118	4.1457	1.0254	0.4387	1.464
After switching	4.0131	4.1487	0.995	0.911	1.906

Table 4.1: Unit-cell parameters of PZT(37/63) calculated from out-of-plane XRD data, before and after switching.

Using the data from Table 4.1 and equation 2.8, the values for ω_{max} can be calculated;

$$\omega_{max(before)} = 2tan^{-1}\left(\frac{4.1457}{4.0118}\right) - 90° = 1.881° \tag{4.1}$$

$$\omega_{max(after)} = 2tan^{-1}\left(\frac{4.1487}{4.0131}\right) - 90° = 1.904° \tag{4.2}$$

Comparing the above calculated values for ω_{max} with the measured values for $\Delta\omega$, it can be seen that after switching the tilt angles for the a- and c-domains seem to be equal to the maximum value based on the lattice parameters. Using equation 2.10 the domain fractions can be calculated based on the tilt angles;

$$\phi_{c(before)} = \frac{1.0254}{1.0254 + 0.4387} = 0.70 \tag{4.3}$$

$$\phi_{c(after)} = \frac{0.995}{0.995 + 0.911} = 0.52. \tag{4.4}$$

Using purely the tilt angles of the domains, a change in domain fraction between the switched and un-switched state is predicted. It appears that upon switching the material, the domain tilt angles are pushed to their maximum value based on the lattice parameters. Upon doing this the domain fractions change.

Another observation is that the splitting of the domain peaks appears to relax back to it's original configuration. Two extra map scans were made with the XRD at a later time, comparing again the switched area to the area that had not been switched. These scans are shown in Figure 4.2. The scans show no clear distinction anymore between an area that has been switched and an area where this did not happen.

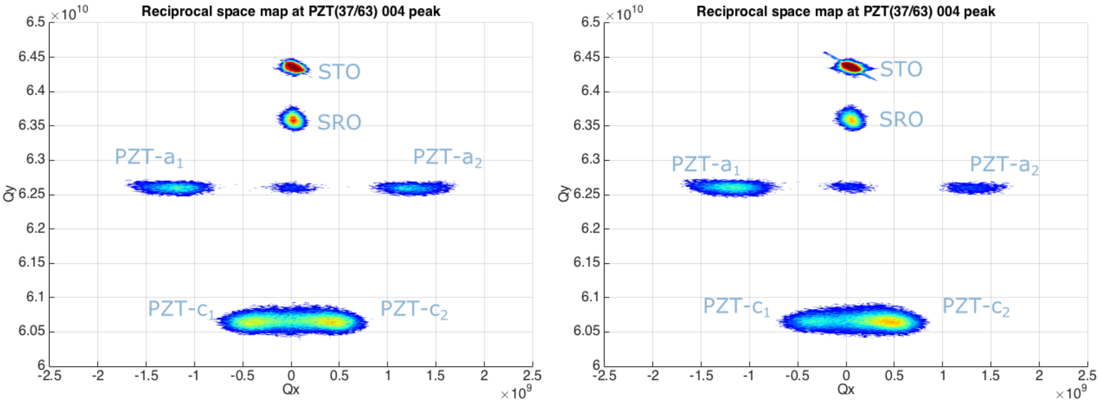

(a) (b)

Figure 4.2: Reciprocal space maps around the PZT(20/80) 004 peaks. Images are from the same areas as in Figure 4.1, only it could not be distinguished which side has switched and which not. The locations for the STO, SRO and different PZT peaks are indicated by the labels in the graphs.

It must be mentioned that the top-electrode, that was put on half of the sample to be able to switch it, was removed prior to the measurement. Because the sample had been etched in a particular way, it could by eye be observed where the region was that divided the two sides of the sample. However, the difference between the switched side and un-switched side could no longer be distinguished. The fact that both scans are more or less the same, still leads to the conclusion that the switched part of the sample somehow relaxed back to it's initial configuration. What drives this relaxation process is unclear, it might be the fact that the sample was put inside the ultra-sonic cleaning bath for 30 minutes. The sample was not heated after the first measurement, but still the relaxation might also be a thermodynamicly driven event.

4.1.2 PZT(20/80)

The same scans as in Figure 4.1 were also made for a PZT(20/80) sample, these are shown in Figure 4.3. For the PZT(20/80) sample the changes are less obvious compared to the PZT(37/63) sample, but also in this case the different c-domain peaks appear to be more well defined after switching.

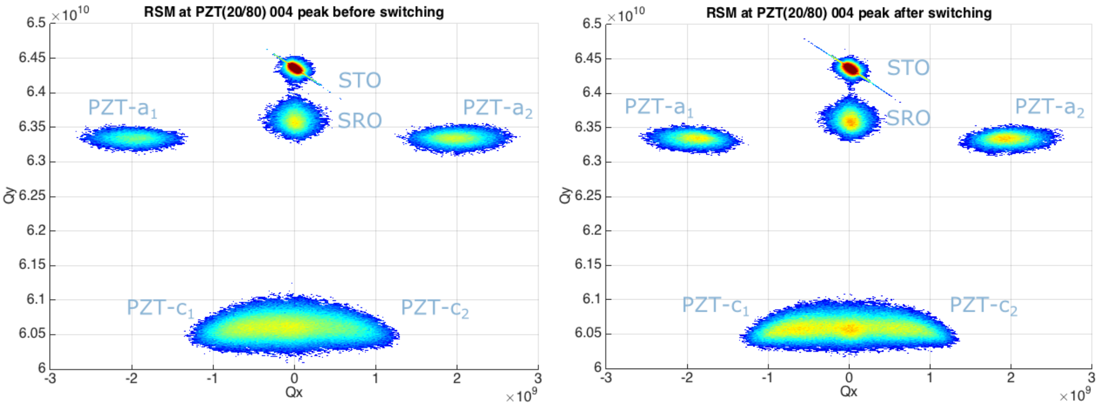

(a) (b)

Figure 4.3: Reciprocal space maps around the PZT(20/80) 004 peaks. (a) initial and (b) after switching the sample a number of times above the coercive field. The locations for the STO, SRO and different PZT peaks are indicated by the labels in the graphs.

Table 4.2 gives the lattice parameters and domain tilt angles that were calculated based on the data from Figure 4.3. It can be seen that the a-domain tilt is somewhat lower after switching and that of the c-domains is a little higher, but these changes are much less dramatic as in the case of PZT(37/63), see table 4.1.

	$a_{(001)}$ (Å)	$c_{(001)}$ (Å)	ω_a (deg.)	ω_c (deg.)	$\Delta\omega = \omega_a + \omega_c$
Before switching	3.9734	4.1470	1.768	0.547	2.315
After switching	3.9668	4.1490	1.707	0.695	2.402

Table 4.2: Unit-cell parameters of PZT(20/80) calculated from out-of-plane XRD data, before and after switching.

Using the data from table 4.2 and again equation 2.8, the values for ω_{max} can be calculated for PZT(20/80);

$$\omega_{max(before)} = 2tan^{-1}\left(\frac{4.1470}{3.9734}\right) - 90^\circ = 2.449^\circ \tag{4.5}$$

$$\omega_{max(after)} = 2tan^{-1}\left(\frac{4.1490}{3.9668}\right) - 90^\circ = 2.572^\circ \tag{4.6}$$

It can be seen that the calculated values for ω_{max} in this case do not match the measured values for $\Delta\omega$. Using equation 2.10, again the domain fractions can be calculated based on the tilt angles;

$$\phi_{c(before)} = \frac{1.768}{1.768 + 0.547} = 0.76. \tag{4.7}$$

$$\phi_{c(after)} = \frac{1.707}{1.707 + 0.695} = 0.71. \tag{4.8}$$

It appears that, based on the tilt angles, the c-domain fraction is a little less after switching compared to the value before switching. However, this change is much less than in the case of PZT(37/63), which was expected looking at the lesser change in tilt angles compared to PZT(37/63).

4.2 Voltage switching experiments in PZT(20/80)

In previous section a difference in the behavior of PZT(37/63) and PZT(20/80) is observed in XRD reciprocal map scans. In section 3.3.1 it is observed that some kind reorienting of the a- and c-domains takes place upon switching the material. In this section the same type of ω-scans are shown on a PZT(20/80) sample, to test if this behavior is also different for PZT(20/80).The resulting ω-scans are shown in Figure 4.4. The data shows no change in intensities of the left and right tilted a- and c-domains before and after switching it on +14 and -14 Volt. It can be seen that after switching the c-domains at -14 Volt the intensity curve changes somewhat, but this seems to be more of an overall intensity drop than a real change in configuration.

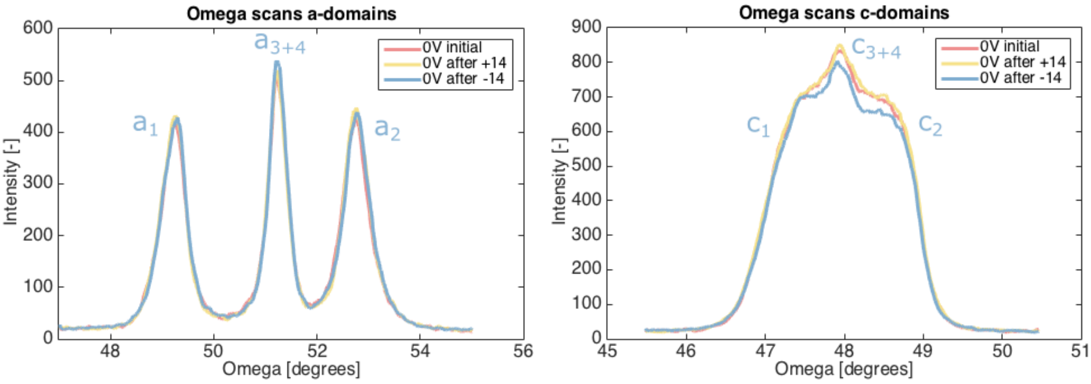

(a) (b)

Figure 4.4: Omega scans of a PZT(20/80) sample at the a-domains (a) and c-domains (b) for three different situations; initial, 0 Volt after switching at +16 Volt and 0 Volt after switching at -16 Volt. The names of the different peaks are given in the graph.

To show what happens when the voltage is applied, in Figure 4.5 the omega scans at 0 Volt are compared to the omega scans at +14 and -14 Volt. The graphs show that the overall intensity of the c-domains becomes larger and of the a-

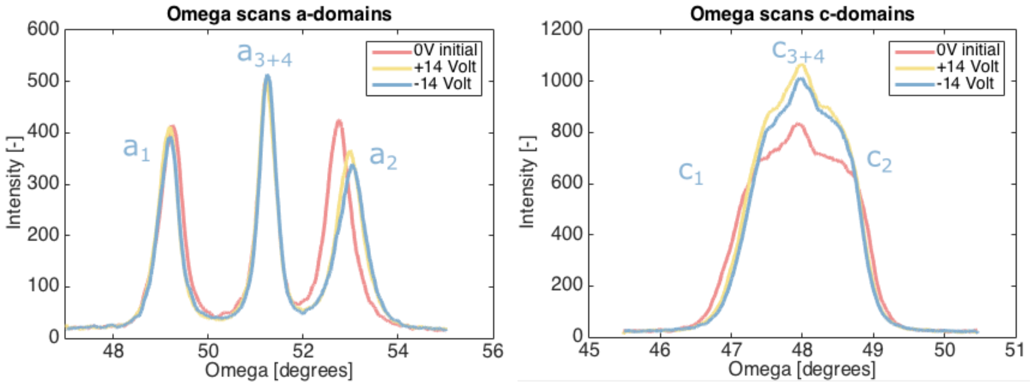

(a) (b)

Figure 4.5: Omega scans of a PZT(20/80) sample at the a-domains (a) and c-domains (b) for three different situations; at 0 Volt, at +14 Volt and at -14 Volt. The names of the different peaks are given in the graph.

domains becomes slightly smaller, this is due to the in section 2.3 treated extrinsic piezoelectric effect.

4.3 Discussion

In section 3.3.1, XRD data is shown from *K. Vergeer* done on a PZT(40/60) sample. Also *R. Steenwelle* used PZT(40/60) together with PZT(20/80) and PZT(45/55) throughout sections of his PhD thesis to show compositional differences in PZT thin films. The question might come to mind as to why this composition was not used for this research. Despite several attempts, it seemed to be impossible to reproduce samples with the PZT(40/60) composition that showed the expected surface domain structure. Although the same PLD target was used, that had been used for successful samples in the past it was not possible to reproduce the same samples. All films grown for this research, using a PZT(40/60) target, showed a kind of grainy surface structure, which is shown in Figure 4.6. In Figure 4.6 the domain structure of a PZT(40/60) sample is still visible, but there is some sort of roughness pattern that distorts the image. A possible reason for this surface pattern might be that the PLD target does not have the right density anymore. Instead of ordering a new target, the possibility was explored to use another composition. After making two samples, a PZT(37/63) and a PZT(43/57) sample it was decided that the PZT(37/63) sample was a good replacement for the PZT(40/60). The results of section 4.1 show that this is indeed the case.

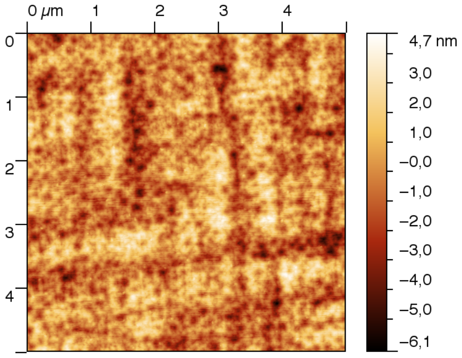

Figure 4.6: AFM surface topography image of an unsuccessful PZT(40/60) sample showing a strange surface roughness.

4.4 Conclusions

The process of domain splitting and relaxation described in section 4.1.1, suggests that upon switching the material above it's coercive field, the c-domain fraction is lowered and the tilt angles for both domains change to match the maximum total tilt angle. This new configuration seems to relax back to it's initial state, which suggests that the original state configuration a lower energy state. Which mechanism drives this relaxation is unclear since for this sample it could have been a couple of factors. Since the top-electrode was partially removed, it could be a depolarizing effect. Although, since some parts of the top-electrodes were still present, this explanations seems rather unlikely. Another explanation to the relaxation process might be the fact that the sample had been in a ultrasonic bath, to remove the top-electrode. Finally it could be a thermodynamic relaxation process driven by finite temperature and time.

Based on the XRD data presented in this chapter, a difference is observed in the behavior of PZT(37/63) and PZT(20/80) both grown under the same circumstances. Where the XRD measurements seem to indicate a movement of the domains in PZT(37/63) upon ferroelectric switching, the domain structure of PZT(20/80) appears to be more fixed. As mentioned earlier in this work, an article by *Su et al.* [19] predicts the complete pinning of the domain wall in PZT(20/80) on misfit dislocations at the film substrate interface. Based on their calculations they dedicate this pinning of a-domains to a combination of the surrounding depolarization field and the stress field at the misfit dislocation-pairs. Data from PZT(37/63) and PZT(40/60) samples shows that for these compositions this pinning can no longer be the case, as explained in section 3.3.1.

The observed difference between PZT(20/80) and PZT(37/63) led to the use of these two compositions throughout this research. PZT(37/63) in this case replaces the more standard used PZT(40/60) composition.

Chapter 5

TEM cross-section analysis

To test the theoretical expectations about the relation between height profile and domain structure in the samples that were made for this research, a cross-section TEM analysis was performed.

5.1 Domain configuration

In section 3.2.4 the sample preparation process is described. The goal of the TEM measurement was to test if the domain configuration was how it is expected from theory and if the height profile that is observed at the film surface is related to the underlaying domain configuration the way it is described in section 2.2.1.

Figure 5.1(a) shows a cross section of the sample where the STO substrate, the SRO bottom electrode and the PZT(20/80) layers are visible. Figure 5.1(b) also contains a gold top-electrode with a platina adhesion layer. The sample that was used, was half covered with a top-electrode which was used to switch this half of the sample. At the time it was thought to also observe a difference before and after switching in PZT(20/80). The expected tetragonal a/c-domain structure is clearly visible, a- and c-domains occur separated by a domain wall that is oriented with an angle of about 45° with the sample substrate. As expected, the a-domains stretch out through the complete film of PZT. Also interesting to note is the vertical grain-like structure that can be observed, which seems to be more chaotic at the SRO-PZT interface, possibly because of dislocations. The PZT wants to grow in a cube-on-cube manner on top of the epitaxial SRO bottom-electrode, but experiences epitaxial stress due to the difference in lattice parameters between both materials. The defects are formed to relax this stress until the film can grow

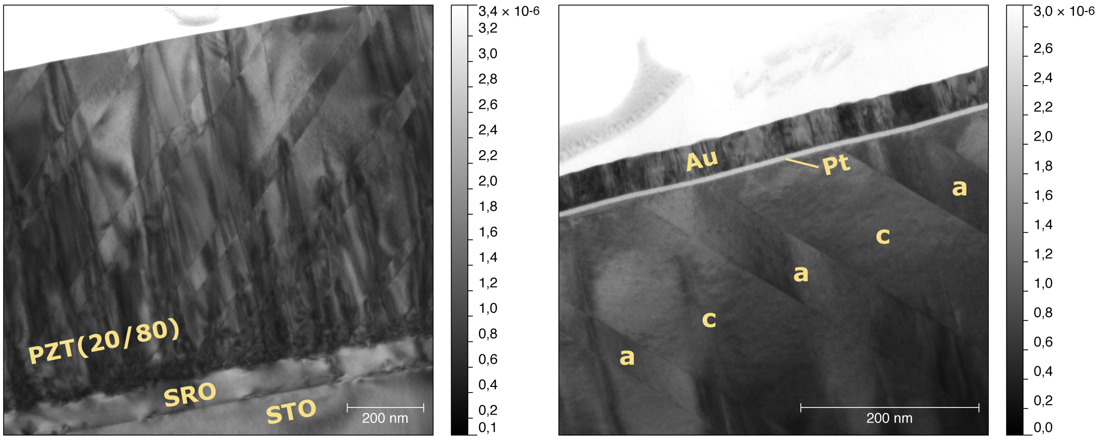

(a) (b)

Figure 5.1: Cross-section TEM images of a PZT(20/80) sample, showing the complete stack of layers (a) and a more detailed image of the surface profile (b).

in a epitaxial manner using more-or-less its bulk lattice parameters.

In Figure 5.1(b) a more detailed image is shown of the PZT surface. The very bright layer on top is the very thin platina adhesion-layer and the more dark layer on top of that is a gold top-electrode. The image confirms the expected relation between the surface profile and the underlying domain structure, the top and bottom locations in the height profile correspond to the location of the domain-walls. This confirms that the domain structure of the film should indeed be observed by looking at the surface of the film.

Figure 5.2(a) shows a TEM image of a domain wall, which partly is enlarged in Figure 5.2(c). It can be seen that the image has atomic-plane resolution, which makes it possible to do qualitative analysis. Figure 5.2(b) shows a 2D FFT analysis of Figure 5.2(a). The dots on the FFT are related to repeating patterns in Figure 5.2(a) and in this case correspond to the crystal planes in the PZT material. It can be seen that there are two distinguishable patterns present in the image, which are separated by a certain angle. The lines in the FFT image are drawn by a program called *gwyddion*, which is used to analyse the images, in this case to calculate angle between the two dots. The coordinates of these lines and the angles between them are summarized in Table 5.1. From the values in Table 5.1 it is calculated that the angle between line 1 and 2 and between 3 and 4 is in both cases 2,4 degrees. The performed FFT analysis using *gwyddion* has a relative high error margin in the ϕ because the analysis is mostly done manually. Taking this error into account this corresponds very well to the ω-offset values from the XRD mapscan analysis in section 4.1.2.

Line	Δx	Δy	ω ± 0.1 [deg]
1	9.89	-0.05	0.3
2	10.39	0.38	-2.1
3	-0.01	10.28	-90.1
4	-0.44	10.00	-92.5

Table 5.1: coordinates from the lines drawn in figure 5.2(b).

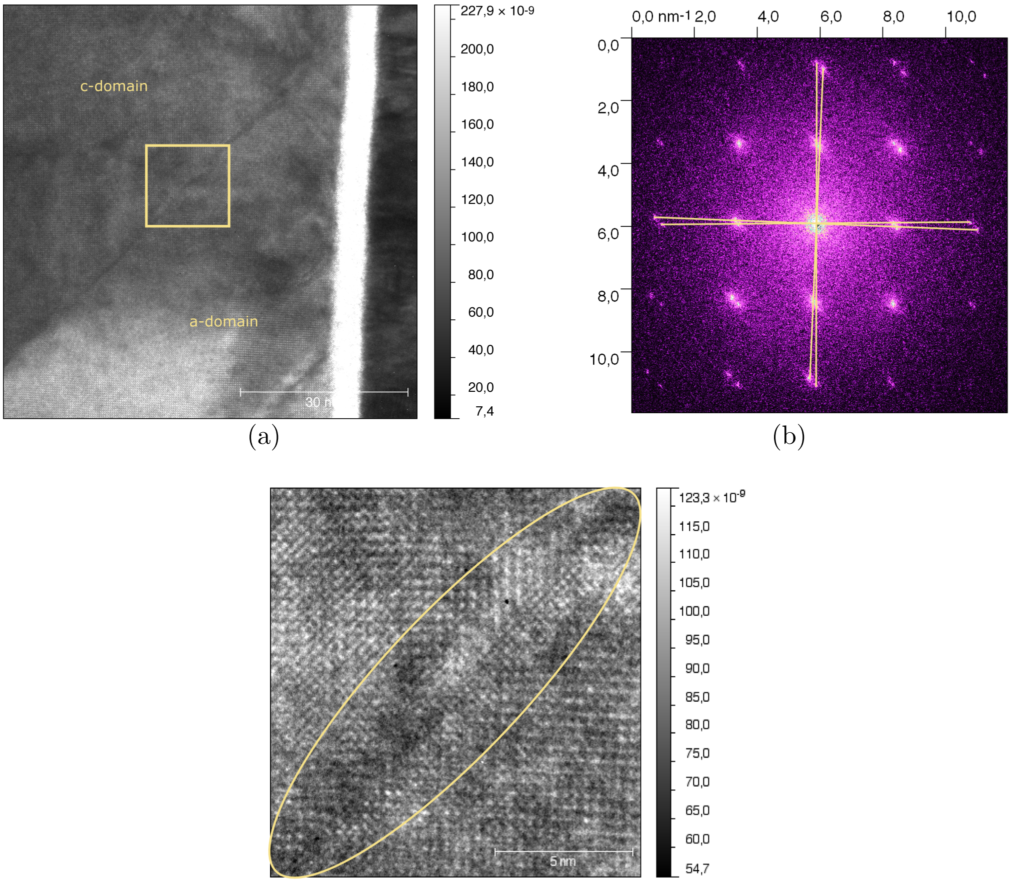

(a)

(b)

(c)

Figure 5.2: (a) Image showing a closer look at the domain wall between a- and c-domains. (b) 2D FFT analysis of the image from (a) The yellow lines are used to calculate the total tilt angle for the a- and c-domains. (c) Enlarged image from the yellow square in (a) showing a closer look at the domain-wall between the a- and c-domain. The area of the domain-wall is encircled in yellow.

5.2 Domain fraction

Besides checking the relation between height profile and domain structure, the TEM images can also be used to calculate the c-domain fraction for the PZT(20/80) sample. As explained in section 2.2, the theoretical domain fraction can be calculated based on the lattice parameters of the thin-film and substrate at high and low temperature. In this section this value is compared to a value that is extracted from the TEM images.

High and low temperature XRD measurements have been performed, giving the unit-cell sizes at 600°C and at room temperature. The measured lattice constants for PZT(20/80) are summarized in Table 5.2.

$d_{1(STO)(600°C)}$	$d_{1(STO)(RT)}$	$d_{1(PZT)(600°C)}$	$a_{1(RT)}$	$a_{2(RT)}$	$c_{1(RT)}$	$c_{2(RT)}$
3.9199	3.9070	4.0277	4.1510	3.9716	3.9916	3.9916

Table 5.2: Unit-cell parameters calculated from XRD measurements at high and low temperature.

Using equation 2.7 and the data from Table 5.2 the c-domain fraction can be calculated;

$$\phi_c = \frac{\left(\frac{4.0277^2 \cdot 3.9070^2}{3.9199^2}\right) - (4.1510 \cdot 3.9716)}{(3.9916 \cdot 3.9916) - (4.1510 \cdot 3.9716)} = 0.669 \tag{5.1}$$

As stated above the domain fraction can also be extracted from the TEM images, this done with the *measure distances tool* in *gwyddion*. Figure 5.2 shows a TEM image with several a- and c-domains. In the image, lines were drawn to calculate the with of the a-domains and the total with of a- and c-domains. Note that the lines are somewhat exaggerated in the image to make them more visible. Because the lines should all be drawn parallel to each other and to the surface, line 1 is drawn to determine the angle of the films surface. All other lines are drawn with more or less the same orientation, see the table in Figure 5.3. To calculate ϕ_c, one simply has to extract all the a-domain with values from the total with, and normalize that;

$$\phi_c = \frac{R_2 - R_3 - R_4 - R_5 - R_6 - R_7}{R_2} = \frac{0.5942}{0.8161} = 0.728 \tag{5.2}$$

This method has been done for several TEM images which are not all printed in this report. Table 5.3 lists the results for these images. In the table, the measured domain fraction is given aswel as the amount of a-domains that was used in the measurement, sinds this is a measure for how good the image represents the bulk value. This method for measuring is pretty accurate for measuring the local domain fraction. However it can be seen that there is quite some difference in the values from different images, which makes sense because the local domain fraction does not necessarily have to be the same everywhere or have to match the value for the complete sample. TEM image number 1 is the one that is calculated using Figure 5.3.

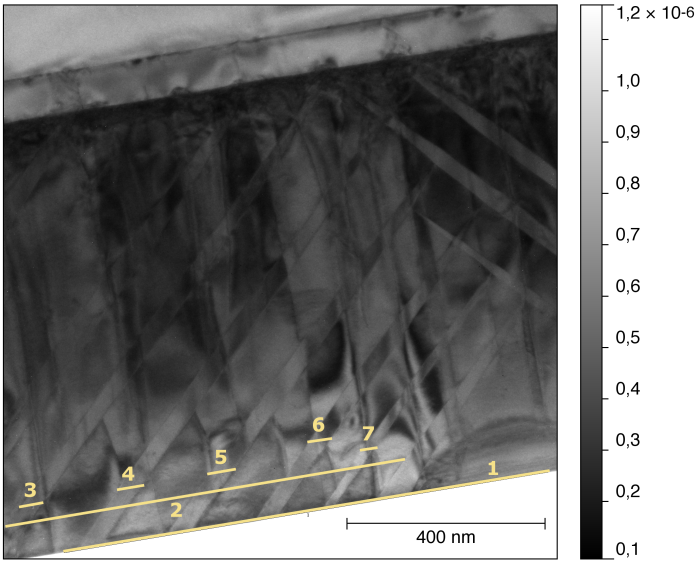

Line	ω [deg]	R[μm]
1	9.5	0.9865
2	9.5	0.8161
3	9.9	0.0449
4	9.8	0.0497
5	9.5	0.0514
6	8.1	0.0451
7	9.5	0.0308

Figure 5.3: TEM image with lines drawn with the 'measure distances' tool in gwyddion. The table contains the coordinates from the lines drawn in the figure.

TEM image	ϕ_c	# of a-domains
Equation 5.1	0.699	-
1	0.728	5
2	0.649	4
3	0.715	4
4	0.735	4

Table 5.3: Calculated value for the c-domain fraction based on equation 5.1 and the measured values from different TEM images.

5.3 Difference in switching and non-switching

As said before in section 5.1, the sample that was prepared for the TEM measurement was partly covered with a gold top-electrode to be able to ferroelectrically switch the PZT(20/80) thin film. The idea behind this was to see if there would be an observable difference in the cross-section images of the PZT thin film before and after switching. At the time it was not yet known that the PZT(20/80) composition was pinned to the film interface and did not show the the behavior of the PZT(40/60) sample shown in section 3.3.1.

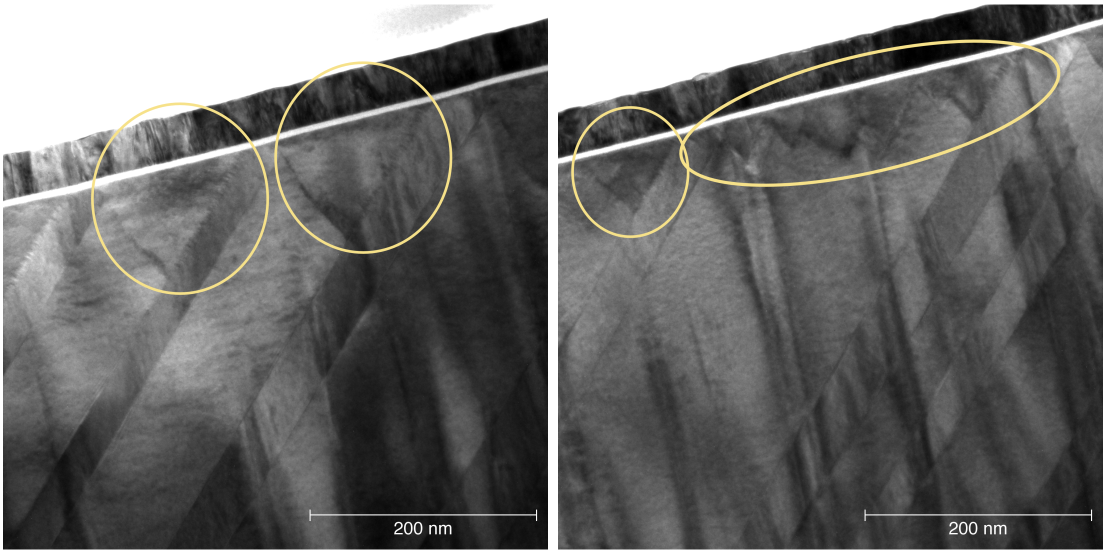

(a)

(b)

Figure 5.4: TEM images taken at the part of the sample that was ferroelectrically switched showing the strange triangular surface pattern. The yellow lines indicate the area's of interest.

However an interesting observation is done on the sample at the region where the gold top-electrode was. Figure 5.4 shows two TEM images taken at the side that was ferroelectrically switched. Both figures show a strange triangular/sawtooth pattern at the PZT-Pt interface. This has not been observed at parts of the sample that had not been switched. What might cause these patterns is unclear, but obviously it has something to do with the ferroelectric switching. Most likely these area's are c-domain areas that have their polarization vector opposite to the direction of the underlying c-domain. When the sample is switched from positive to negative voltage, the c-domains are expected to change their polarization vector according to this voltage change. It somehow looks like if after the voltage was removed some of the c-domains changed their polarization to another state than the c-domains that are below them. A reason for this might be the depolarizing field from the top-electrode, which also would explain why this only happens at the surface.

5.4 Discussion

The measured domain fraction from the TEM images does not seem to match the domain fraction that is calculated based on XRD temperature measurement data. To get more data on the domain fraction for a 20/80 sample, ω-χ-scans were done on the XRD, scanning through the a-domain plane and the c-domain plane of the out-of-plane 002 peak. The data from these scans allows one to measure the intensities for both domains, which also after correction for the structure factor gives the domain fractions. Based on these measurements the c-domain fraction was determined at 0.673 for a PZT(20/80) sample, which is actually really close to the in this chapter calculated value of 0.669.

It is hard to say exactly to what this difference can be accounted, but the most likely reason is the fact that one dimension of the crystal is practically completely removed during the preparation process. In order to make a TEM image, the crystal has to be transformed into a very thin electron transparent slice of material. This means that the film is no longer strained in one of the two directions, and upon heating it is likely to find a new domain configuration. After gluing of the samples the sample is heated at about 120 degrees, which might already be enough. This heating during the preparation process can be bypassed by a different preparation process called Focussed Ion Beam Milling, however this has not been tested during this research because of budgetary reasons.

If however the restructuring towards a 2D crystal is the reason for the domain fractions to not match the theory, this means that the film is going from an a-, b- and c-domain structure towards a more or less purely 2D a- and c-domain structure, this could be calculated using more or less the same equation but then calculated not for area but for a line. One would get the following equation;

$$\phi_c = \frac{\left(\frac{d_{1(PZT)(600^\circ C)} \cdot d_{1(STO)(RT)}}{d_{1(STO)(600^\circ C)}}\right) - a_{1(RT)}}{c_{1(RT)} - a_{1(RT)}} = \frac{\left(\frac{4.0277 \cdot 3.9070}{3.9199}\right) - 4.1510}{3.9916 - 4.1510} = 0.857 \qquad (5.3)$$

This does also not agree the measured values in this chapter.

It could also be argued that all the b-domains that were present in the sample just become c-domains without completely restructuring the sample. This would in theory mean that half of the so to say non-c-domains also becomes a c-domain.

The domain fraction would then be;

$$\phi_c = \phi_c + \left(\frac{1-\phi_c}{2}\right) = 0.699 + \left(\frac{1-0.699}{2}\right) = 0.849 \tag{5.4}$$

This gives more or less the same value as the previous calculation.

Because the process of sample preparation and sample analysis in TEM is quite expensive, only a TEM measurement was done on a PZT(20/80) sample. This means that making a comparison with a PZT(37/63) sample, as is done throughout this thesis, was not possible. It is however expected that a PZT(37/63) shows the same kind of structure but then with a different domain fraction and domain angling.

5.5 Conclusions

The images resulting from the TEM measurement clearly showed the a/c-domain configuration that was expected to be present in the PZT thin films grown on a STO substrate. The presumption of a 45 degree oriented domain was was also confirmed by the TEM images. High Resolution TEM images showing the crystal planes inside the thin films were analyzed and confirmed the previously calculated angling of about 2,4 degrees between the a- and c-domains.

The TEM images show a clear relation between the thin film surface profile and the underlying domain structure. This is an important conclusion for this research because if this would not have been the case, it would not be possible to probe the domain structure using an AFM. Figure 5.1(b) shows that the location of the domain walls correspond with the minima and maxima in the surface profile.

The domain-wall that exists between the a- and c-domains can also be observed in the high resolution TEM images. It is observed that a domain changes within one or two unit-cells into the other type of domain, without the observation of a significant area of defects in between. This indicates that the domain-walls in the PZT(20/80) sample that was used are in the order of one or two unit-cell sizes thick. However one must always keep in mind the fact that the sample is more-or-less completely stress-free in one of the three crystal dimensions, which is a unique situation and does not necessarily mean that this is also the case in a regular three dimensional crystal.

Chapter 6

Mapping the domain structure

6.1 Scanning probe surface analysis

6.1.1 Atomic force microscopy

To test the theoretical predictions about the surface profile of the PZT samples, AFM measurements were done on PZT samples without top-electrode. Figure 6.1 shows the typical surface patterns of a PZT(20/80) and a PZT(37/63) sample measured with an AFM. The straight domain patterns are clearly visible and to align with the (100) and (010) orientations of the cubic STO substrate, note that the sample is oriented about 45 degrees during the AFM scanning process.

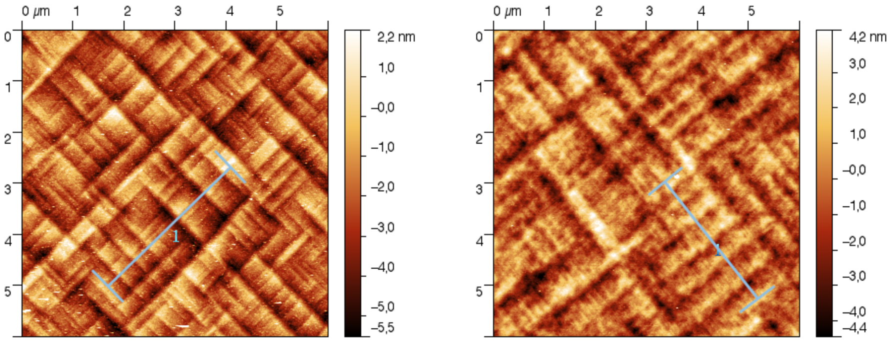

(a) (b)

Figure 6.1: AFM surface profile images of two different PZT compositions (a) PZT(20/80) (b) PZT(37/63). The blue lines in the figure are indicate the location of the height profiles in Figure 6.2.

In Figure 6.2(a) height profiles of the two samples are plotted, made at the lines visible in Figure 6.1. The height profile is averaged over a certain whith, represented by the perpendicular lines in Figure 6.1. The height profiles display the expected straight triangular like shape predicted in section 2.2.1, this has also been reported in the PhD thesis of R. Steenwelle [4].

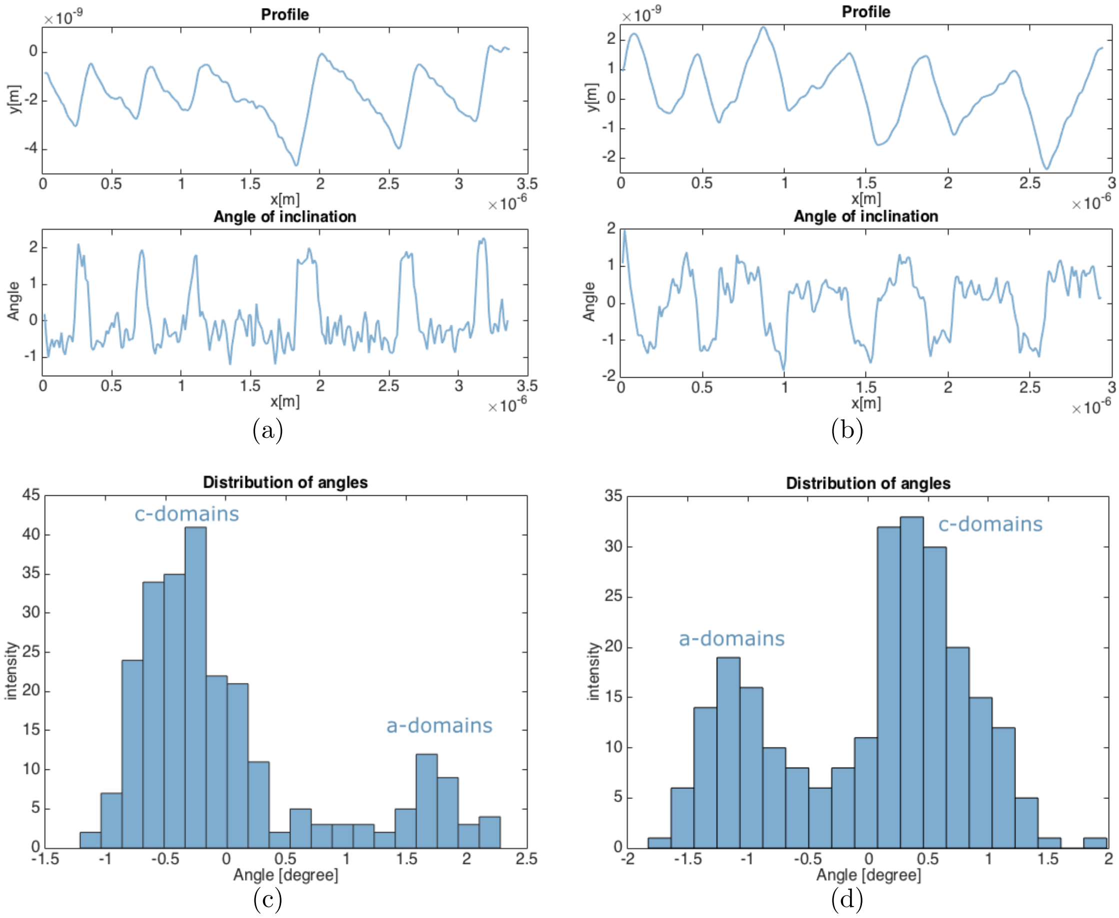

(a)

(b)

(c)

(d)

Figure 6.2: Height profile lines for (a) the PZT(20/80) sample and (b) the PZT(37/63) sample. Also the distribution of angles is plotted for (c) the PZT(20/80) sample and (d) the PZT(37/63) sample.

In Figures 6.2(a) and 6.2(b) also the derivative of the slope is plotted, giving the angle of inclination. It can be seen that there is a clear separation of two levels, in both compositional cases. Theory predicts, based on the unit cell sizes and misfit strain, that the c-domains should be the majority and thereby are the ones with the lower angle of inclination, see equation 2.7. To further clarify the separation of two distinct levels, the distribution of angles is plotted as histogram in Figures 6.2(c) and 6.2(d).

Comparing the ω-values measured with the XRD in section 4.1 to the angles measured with the AFM it can be seen that they match quite well. With the AFM analysis it is pretty hard to give an exact value based on the plotted histograms. Nevertheless the values for PZT(20/80), ω_a=1.745 and ω_c=0.647, match the maximum values in the histogram. Also the PZT(37/63) ω-values for the un-switched state, ω_a=1.025 and ω_c=0.4387, match with the data from the histogram. These conclusions give an indication that it is indeed the a/c-domain structure of the PZT that causes the height profile that is measured with the AFM.

6.1.2 Piezoresponse force microscopy

The relation between surface topography and the underlying domain structure can also be tested using a PFM measurement. Figure 6.3 shows an in-plane amplitude and phase image together with the corresponding height profile of a PZT(20/80) sample. Although the height image from a PFM measurement is not as sharp as would have been when measured with a *tapping mode in air* AFM-setup, the plotted height profile, which is made at the line drawn in Figure 6.3(c), still displays a sawtooth shaped surface profile that was also measured with the AFM.

The amplitude image of Figure 6.3(a) shows clear in-plane polarized areas, so called a-domains, at the locations where in Figures 6.3(c) and 6.3(d) the slope is the steepest. This is what would be expected from the theory and the calculated domain fractions. The phase image in Figure 6.3(b) shows a contrast between two pieces of in-plane polarized domains at the bottom of the image and the rest of the in-plane domains, this is because these two domains have their polarization vector 180° opposite to the rest of the in-plane domains in the figure.

The PFM measurements confirm the expectations about the relation between the surface profile and the underlying domain structure for a PZT(20/80) sample. No PFM measurements were performed on a PZT(37/63) sample, but measurements performed in the past show similar behavior to the PZT(20/80) sample [4].

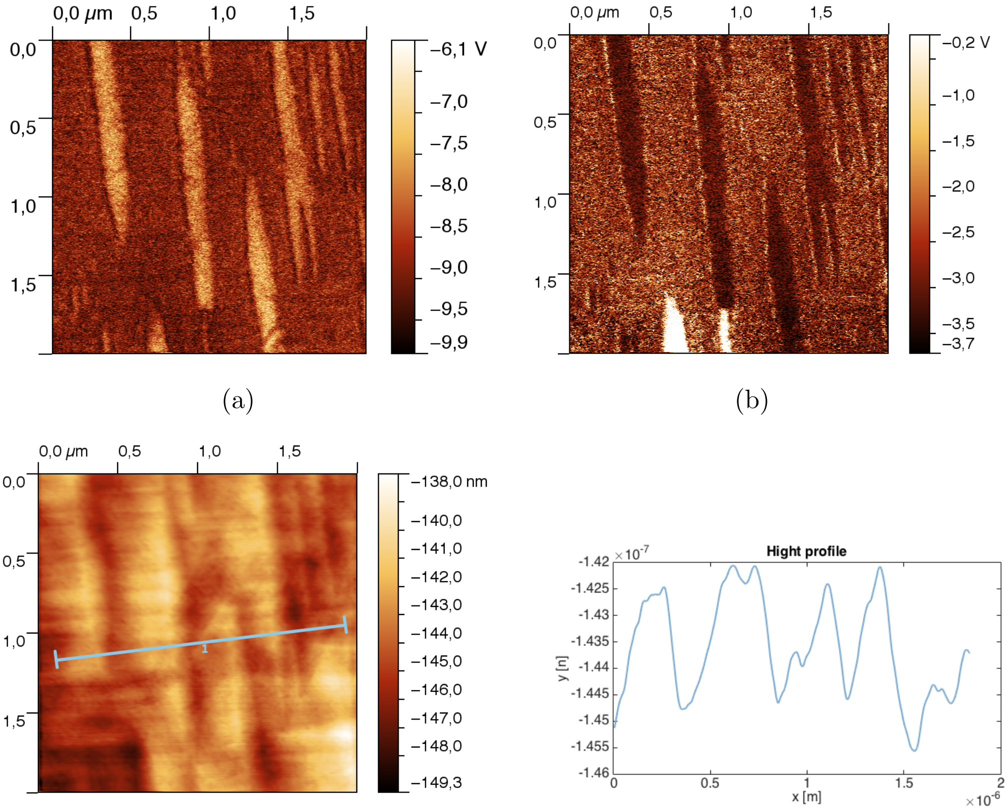

(a) (b)

(c) (d)

Figure 6.3: PFM images of a PZT(20/80) sample. (a) In-plane amplitude, (b) in-plane phase, (c) height image and (d) height profile taken at the blue line in (c).

6.2 Sub-domain pattern

The AFM images shown in this chapter show, besides the studied a/c-domain structure, another smaller surface pattern in both compositions. Perpendicular to the a/c-domain structure, small lines can be observed that look like kind of a rippling effect of the c-domain. Figure 6.4 shows enlarged images for both compositions where these structures can be observed.

It is likely that the observed pattern has something to do with stress relaxation perpendicular to the local a/c-domain structure. As explained in the theoretical section, the domains are formed to relax stress imposed by the substrate. Since also b-domains are needed to relax the other in-plane stress, locally this might be a problem when the a- and c-domains are relatively long. This means the small

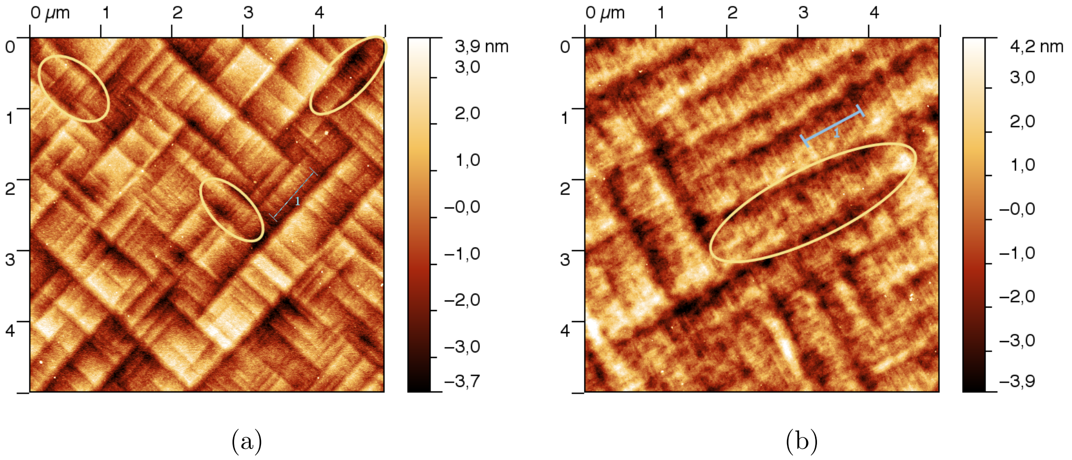

Figure 6.4: $5\mu\times5\mu$ AFM scan of (a) PZT(20/80) and (b) PZT(37/63) sample. The scans show the observed smaller surface patterns perpendicular to the a/c-domains. The blue line in (b) indicates the location of the height profile that is used in Figure 6.5. The yellow encircled areas are areas where the pattern can be observed.

patterns could be domains that are needed to relax stress in the length direction of the domain. If this is the case, it is expected that these domains would have a different crystal structure which could be observed using XRD or PFM. It is also expected that the domain structure would exist throughout the complete thickness of the film, this because otherwise it would not relax any stress at the substrate-film interface. Another scenario could be a ripple effect occurring only at the film to air interface. A phenomena like this has also been observed in the pas for another perovskite material [18]. This would mean that there would be no observable difference in crystal structure, and that the phenomena would not be throughout the complete film thickness.

When the same AFM analysis is done on these patters as done on the larger surface domain structure, no clear separation into two distinct levels is observed, see Figure 6.5. However, at the length and height scale of these small ripples, it is the question whether the AFM can accurately measure the slope of these patterns. The analysis is done on the PZT(37/63) sample, see the blue line in Figure 6.4(b), for the PZT(20/80) sample the results were exactly the same.

To test if the patters are domains with different orientations, PFM measurements were done to probe the piezo-response of the surface and thereby tell something about the polarization at the surface. In Figure 6.6 the out-of-plane images of the same PFM measurement as Figure 6.3 are shown. The phase and amplitude clearly show a response to the cantilever at the places where the surface profile is visible on the height profile. Note that the height image of a PFM measurement

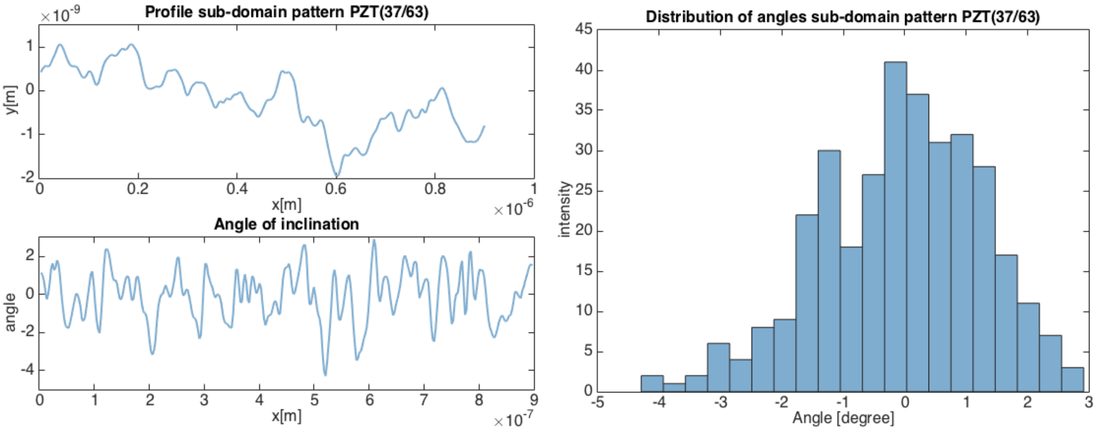

(a) (b)

Figure 6.5: Height profile (a) and distribution of angles (b) for the sub-domain pattern of the PZT(37/63) sample from Figure 6.4(b).

is by far not as accurate as a typical *tapping mode in air* AFM measurement. As explained in section 3.2.2 the response on an out-of-plane PFM measurement could also arise from an in-plane polarized section that is in the direction of the cantilever, which is the case for the horizontal lines in Figures 6.6(a) and 6.6(b). This way it could be concluded that the small surface patterns are small in-plane polarized domains, occurring only on the out-of-plane c-domains of the regular domain structure.

However, if this smaller pattern would be an extra in-plane domain structure, more or less through the c-domain that is already there, one would expect the domains to show up in XRD ω-χ-scan. Since the domains would be on the region of the c-domain, a ω-offset would already be there. In order to fit the new in-plane domains to the out-of-plane structure that is there, both structures would require a new in-plane tilt but than in the χ-direction, perpendicular to the ω-offset. This offset in both ω and χ has never been observed in any XRD ω-χ-scan. The fact that it didn't could also be accounted to the coherency length of the XRD setup which means that the structures that are to be observed do are too small for the setup to distinguish. Figure 6.7 shows an ω-χ-scan for a PZT(37/63) sample. The c-domain peak, in the case where the sample has not been switched, appears as one big blob with a relatively large spread in the χ-direction. This spread in the χ-direction is a consequence of the XRD source. Because this large spread in the data and the coherency problem, it is not possible to draw conclusions regarding the nature of the sub-domain structure based on the XRD data.

Another way of mapping different unit-cell orientations at the surface of a film

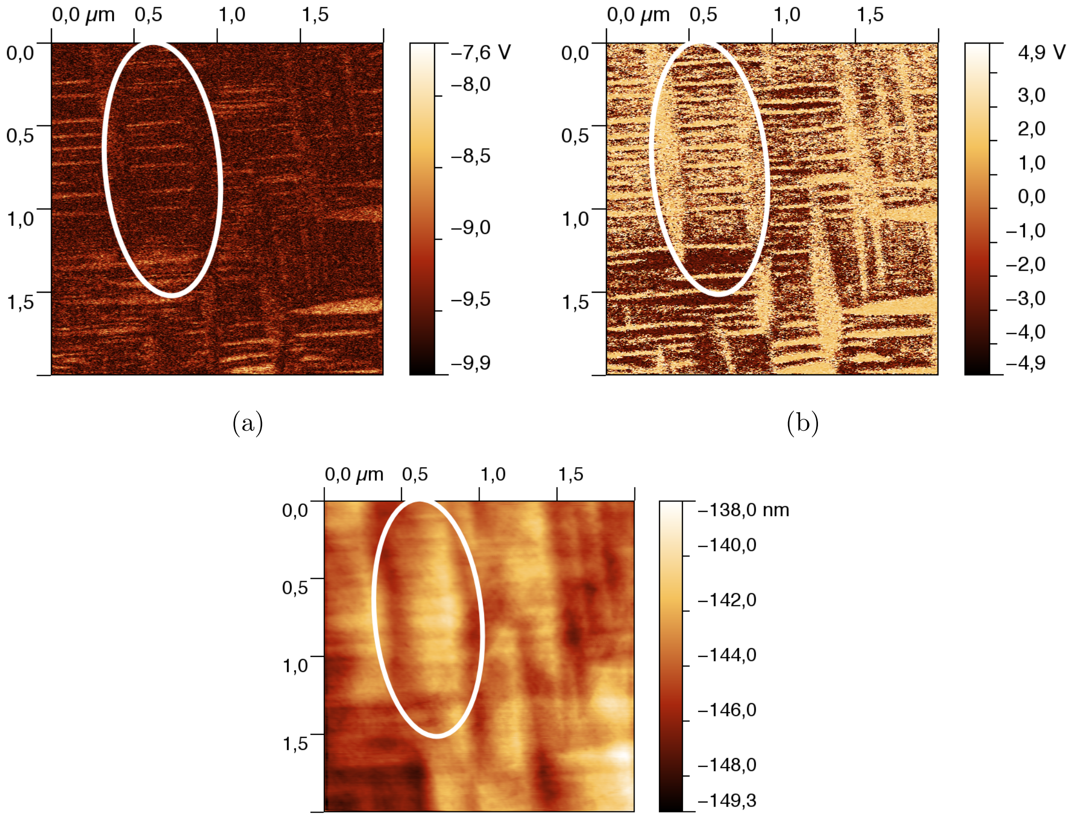

(a)

(b)

(c)

Figure 6.6: PFM images of a PZT(20/80) sample. (a) out-of-plane amplitude, (b) out-of-plane phase and (c) height profile. The white circle indicates an area where the sub-domain pattern can be observed.

is a technique called *Electron backscatter diffraction* (EBSD), which is a operating mode of a *Scanning electron microscope*. With this technique electrons are shot at the sample at a relative low angle of about 30°, this way some of the electrons are able to backscatter and escape the sample. Just like in XRD measurements, the angle at which the electrons leave the sample fulfills the Bragg condition related to the spacing of the lattice planes of the crystalline structure. The scattered electrons collide with a phosphor screen to give what is called a *Kikuchi pattern*, which can be analyzed on the computer. The advantage of this technique over XRD is the fact that a relative small bundle is used to fire electrons, which makes it possible to make a map of the domain structure. Several EBSD measurements were done on a PZT(20/80) sample, unfortunately without any result. The resolution of the SEM was very close to the dimension of the patterns that were analyzed, which made it impossible to distinguish different lattice orientations at the surface. Also drifting

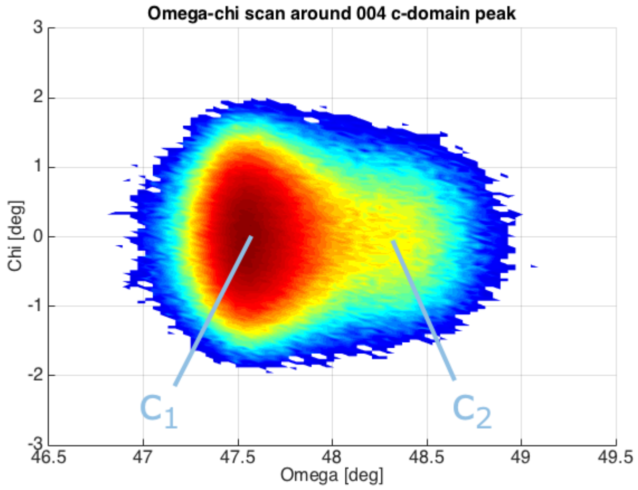

Figure 6.7: ω-χ-scan around a 004 c-domain peak of a PZT(37/67) sample. The two different diffraction spots for the c-domains are indicated in the image.

of the sample during measurement-time was an important factor which might have influenced the accuracy of the measurement.

An explanation to the in-plane piezoresponse measured in the PFM measurement, and the missing domain structure in the XRD measurements could be a buckling effect of the surface. This might be something like the ripple of a piece of paper when it is contracted along the sheet direction. If this is the case, for instance to relax some of the stresses at the films surface, the PFM tip might experience a relative high electric field (or polarization?) close to a local minimum compared to a local maximum of the pattern because the electric field would be stronger there. Because this effect would only be expected at the surface of the film, it is not likely to show up in the performed XRD measurements because a very large part of the sample is probed by the X-rays.

6.3 Discussion

Despite the effort that was put into understanding the smaller sub-domain surface pattern, no clear conclusions can be drawn about the nature of these height variations. The XRD data does not show double tilted in- and out-of-plane domains, but that might also be accounted to the fact that the tilt angle is to small for the XRD to distinguish from the other peaks. Also the volume of the PZT might be too small to show up in the XRD data as a clear distinguishable peak. The PFM data clearly shows a different, in-plane, piezoresponse for the small pattern compared to the out-of-plane domain it is located on. The only other explanation to this effect, besides in-plane domains, is a buckling effect of the surface. With the performed experiments it was not possible to give a decisive answer with regard to the cause of the observed small surface pattern.

6.4 Conclusions

Looking at Figure 6.1 one can see that there is a clear difference in surface topography between the two tetragonal compositions. The PZT(20/80) sample shows very clear and straight pattern while the PZT(37/63) sample shows a more distorted pattern. Nevertheless, both samples show a clear a/c-domain surface roughness pattern that is expected from the theory. The observed domain structures in tetragonal PZT shows twinning like patterns with different angles for a- or b-domains rather than for c-domains. This different angle is caused by the difference in domain fractions which is caused by the difference in unit-cell size [checken].

Comparing the AFM topography data to the measured ω-offset values from XRD measurements, it is concluded that they match quite well. This indicates that the observed topography pattern is indeed related to the underlying domain structure, as was expected from the theory.

Chapter 7

Mapping the domain dynamics

To study the dynamical behavior of the a/c-domain structured tetragonal PZT thin films, *in-situ* ferroelectric switching was done during AFM measurements. Like in the previous sections PZT(37/63) and PZT(20/80) samples were used. Based on the observations from chapter 4 it is expected to observe movement of the domain walls in a PZT(37/63) sample and pinning of the domains in a PZT(20/80) sample.

The samples were put inside the AFM and connected to the measurement setup. To make sure the scans were performed on exactly the same location as the scan before, a landmark was picked in the form of a particle. The AFM tip was withdrawn every time the voltage was applied on the sample, this because the fast piezoelectric response of the samples might otherwise damage the AFM tip.

The samples that were used consist of the following stack of materials; STO/SRO /PZT/Ti/Pt. The process of making the samples is described in full detail in section 3.1.

7.1 PZT 37/63

In Figure 7.1 a series of *in-situ* ferroelectric switching AFM measurements are shown. With the ferroelectric tester the coercive field of the sample was determined at about 5 Volt, depending on the switching speed, therefore the measurement setup was set at a switching voltage of 7 Volt. In the caption of the image the indication 0^{+}V means that it is at 0 Volte after it was switched at +7 Volt.

It must be noted that the images that were taken at -7 Volt are more blurry than the other pictures. This is most likely because the AFM tip experiences some kind of screening effect from the negatively charged top-electrode. Why this is not the case for a positive applied potential has to do with the fact that the tip is made of negatively doped silitium.

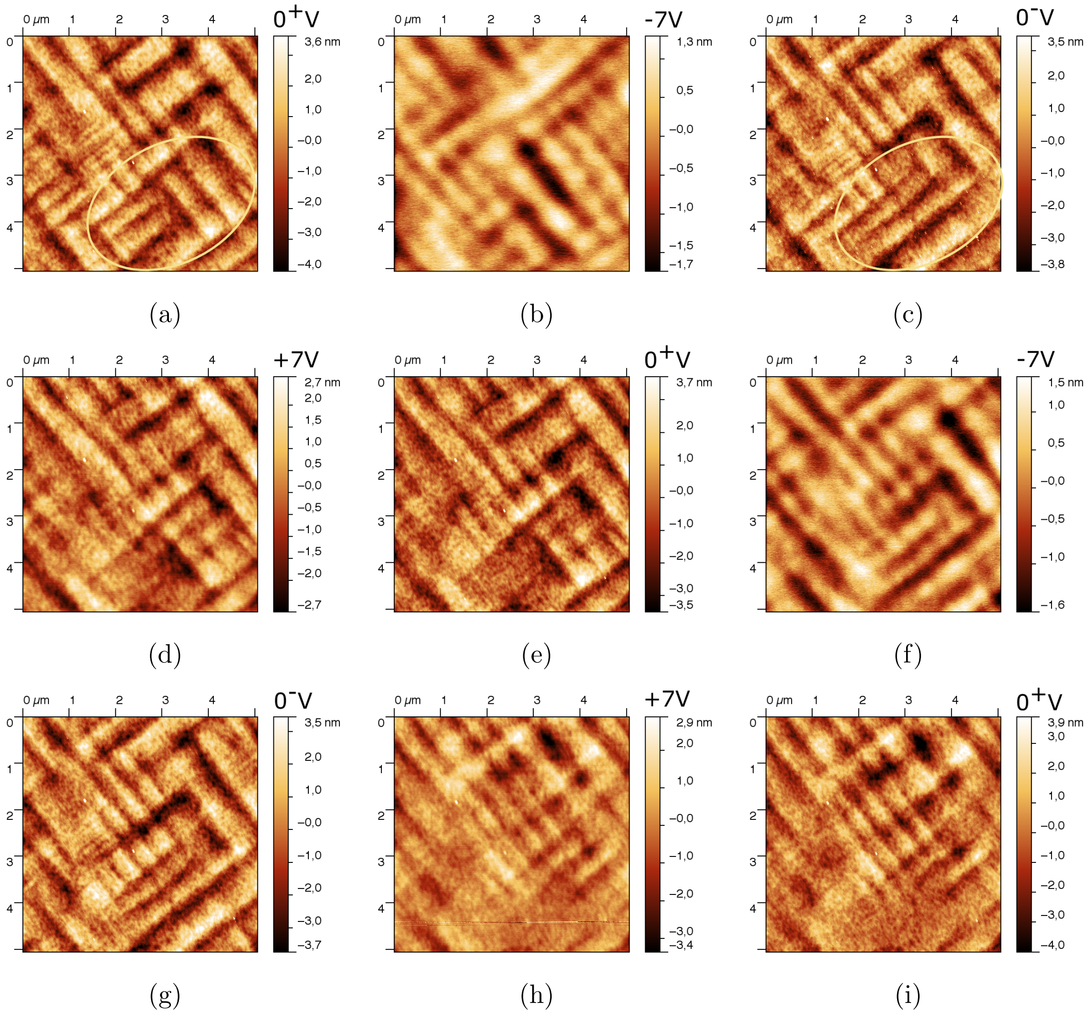

(a) (b) (c)

(d) (e) (f)

(g) (h) (i)

Figure 7.1: Series of AFM pictures taken from a PZT(37/63) sample at different situations (a) 0^+V (b) -7V (c) 0^-V (d) +7V (e) 0^+V (f) -7V (g) 0^-V (h) +7V (i) 0^+V. The yellow lines in (a) and (c) indicate an area that changes upon switching. Note that the location for image (b) is a bit more to the top-right compared to the other images.

The images show that the domains, that are observed via the height profile, change their configuration upon switching. Looking at Figures 7.1(a) and 7.1(c) it can be seen that the domains on the bottom-right, encircled in yellow, are now elongated. Looking at Figure 7.1(e) it can be seen that the domains changed back to their configuration of Figure 7.1(a). This builds the presumption that the domains are switching between two different configurations. However, comparing Figure 7.1(i) to Figures 7.1(a) and 7.1(e), it is concluded that they actually don't match. The fact that Figure 7.1(i) is also different to Figure 7.1(g) indicates that the configuration still changed, but not back to it's so to say initial state. A strong conclusion can unfortunately not be made about this because the images become unclear and it becomes tough to observe the domains. Not that the sample had already been switched inside the ferroelectric tester before the AFM measurement.

Another interesting thing to notice is the fact that there is no difference in domain structure between the images where the voltage is applied to the images at 0 Volt. This indicates that there is no movement of the domains at the point where the voltage is put back to zero. When the voltage is applied the domains restructure and when that voltage is removed, the domains stay that way. In Figure 7.2 data is plotted from an XRD measurement performed by *K. Vergeer*, ω-scans of the a-domains were made at different voltages comparable to the measurements from section 3.3.1. The area of an a-domain peak, expressed in counts, is related to the amount of a-domains that are tilted to that side. The scan shows a hysteresis like behavior, which is expected if the above stated argument about the domain switching is correct. The overall a-domain count is expected to decrease when the voltage is increased, this is explained in section 2.3. Upon reaching the materials coercive field, in this case about positive and negative 4 Volt, suddenly a significant amount of a-domains disappear or appear thereby indicating a reconfiguration of the domain structure.

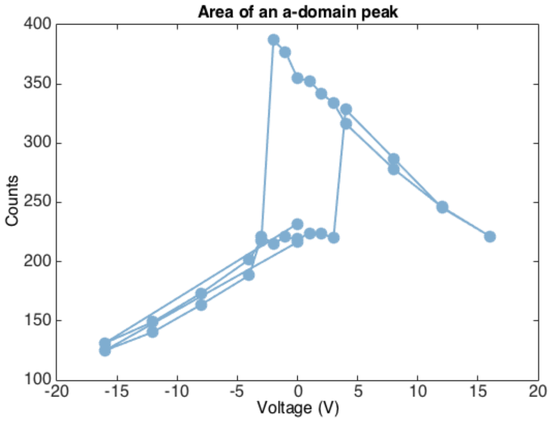

Figure 7.2: Plot showing the change in area of an a-domain peak in an XRD ω-scan when different voltages are applied. Scans have been performed on a PZT(40/60) sample.

In Figure 7.3 the same experiment as in Figure 7.1 is done but this time a larger area is scanned and the scans are only made at $0^{+/-}$ Volt. The images show again a change in configuration of the domains, but in this measurement it becomes clear

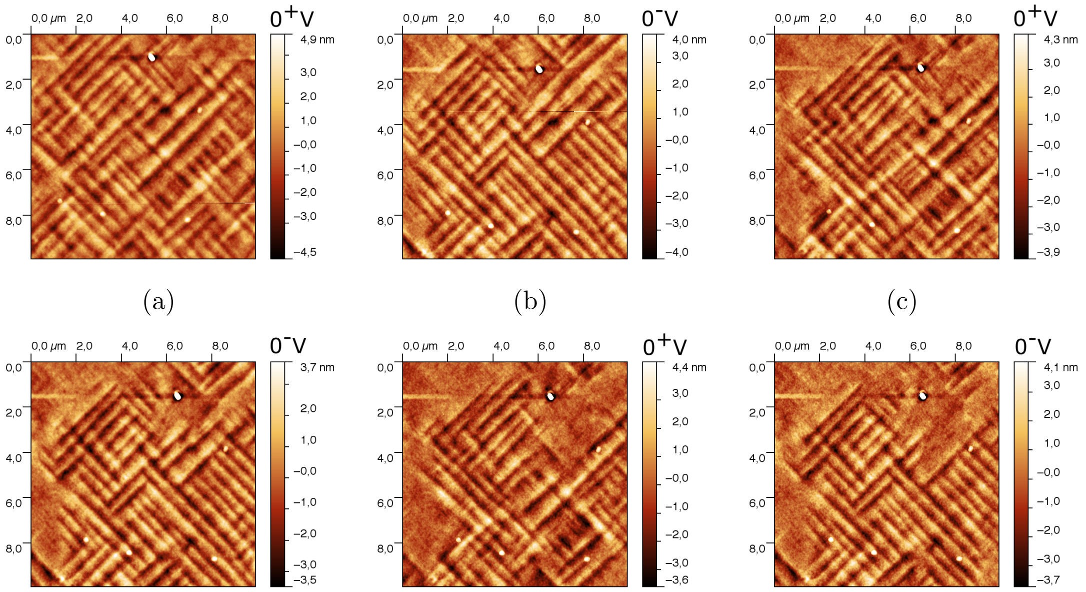

(a) (b) (c)

(d) (e) (f)

Figure 7.3: Series of $10\mu \times 10\mu$ AFM pictures taken from a PZT(37/63) sample at different situations (a) 0^{+}V (b) 0^{-}V (c) 0^{+}V (d) 0^{-}V (e) 0^{+}V (f)0^{-}V. The sample was switched at a voltage of positive and negative 10 Volt.

that the top-electrode layer is less flexible than expected. The images where the sample is switched to the negative side show a much clearer domain configuration than the images where the sample is switched to the positive side. It is expected that the top-electrode layer was deposited on the sample at the configuration which was associated with the negative switched side, and upon switching to the positive voltage to some extend it still holds to that configuration. In other words, the top-electrode is not able to completely follow the height changes due to the underlying domain reconfiguration, as the sample gets switched over and over the metal has more problems following the profile. This can be seen in the left-top corner of the images. Unfortunately this makes it very hard to do further quantitative analysis to the domain reconfiguration. It would be interesting to investigate the way the domains move or restructure, for instance by looking at the angles of the domain patterns as is done in chapter 6.

7.2 PZT 20/80

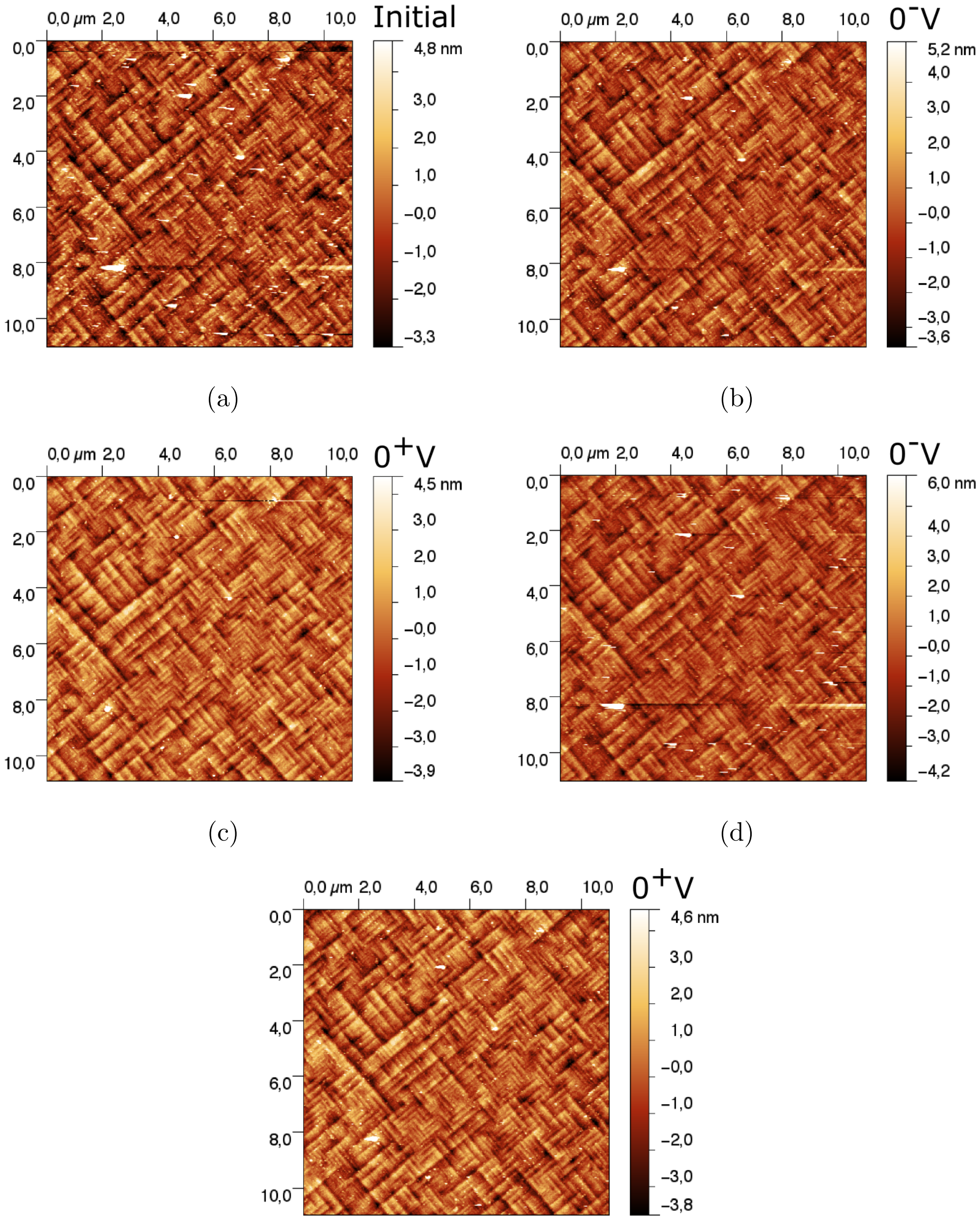

(a) (b) (c) (d) (e)

Figure 7.4: Series of $11\mu\times 11\mu$ AFM pictures taken from a PZT(20/80) sample at different situations (a) it's initial state (b) 0^{-}V (c) 0^{+}V (d) 0^{-}V (e) 0^{+}V. The sample was switched at a voltage of positive and negative 10 Volt.

To test the predictions about the pinning of the domains in a PZT(20/80) sample, an *in-situ* ferroelectric switching AFM measurement was also done on a PZT(20/80) sample. The results of this experiment are shown in Figure 7.4. It must be said that the pictures look contaminated, there seem to be a lot of particles on the sample. As long as the domain structure is visible the amount of particles on the scan area is not really a problem. With the ferroelectric tester, the coercive field of the sample was determined at about 7 Volt, depending on switching speed. To be sure the PZT thin film was ferroelectrically switched with a switching voltage that was set at positive and negative 10 Volt.

Figure 7.4(a) shows the initial state of the sample, this is the state where it has not yet been switched at all. It can be seen that the surface profile does not change in any way when the sample is ferroelectrically switched. The complete series of pictures confirms the presumption that a PZT(20/80) thin film grown on a SRO buffered STO substrate experiences pinning of the domains. Another observation is the fact that the top-electrode layer does not seem to degrade the way it does in a PZT(37/63) sample. This has also been tested after switching the sample 250 times in the ferroelectric tester, even then the top-electrode still showed a complete surface profile of the PZT(20/80) domain structure.

7.3 discussion

As can be seen in the images from Figures 7.1 and 7.3 there appear to be more blurry areas on the PZT(37/63) sample after the sample is switched over and over. It seems that the metal top-electrode layer detaches from the sample as the sample is switched. After switching the sample 250 times in the ferroelectric tester the domain structure even seemed to be gone completely, this is shown in Figure 7.5. It can be seen that the domain structure is completely replaced by a more or less flat surface structure that seems to be divided into separate regions.

This phenomena might be explained by the fact that the moving domain structure pushes the top-electrode loose. The metal layer is thin enough to be flexible to some extend, but it is imaginable that at one point it will not follow the changes in the domain surface pattern anymore. This idea is also supported by the fact that no degradation of the top-electrode is observed in any of the PZT(20/80) samples, where the domains appear to be pinned and thereby do not move.

Several attempts have been done to solve the degradation of the top-electrode. When the phenomena was first observed, gold was used as top-electrode. Different sputtering machines have been tried to see if this influenced the attachment of the layer, without succes. Also depositing a platina top-electrode layer with PLD was

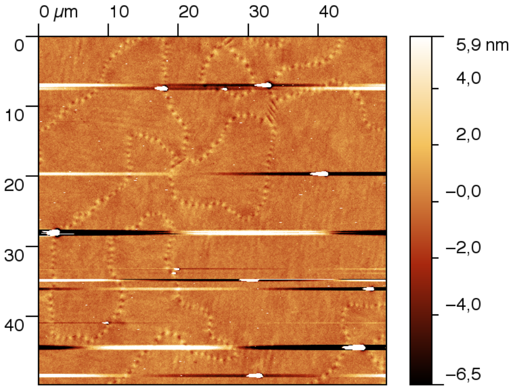

Figure 7.5: AFM image of a PZT(37/63) sample after switching the sample a significant amount of times in the ferroelectric tester. The black-white stripes are measurement errors due to the relative large particles that occur in the image.

tried, this because the sticking of the atoms to the surface should then be much better. However, after depositing the platina no top-electrode could be observed at the surface. Probably the fluency of the setup did not match the desired 5.0 J/cm^2 which is needed to form a good platina plasma. Also the use of a SRO top-electrode has been tested in an early stage of this research, unfortunately for only 10 nm this layer did not grow smoothly, this roughness was due to the initial grain like growth of SRO. Eventually it was chosen to use Platina instead of gold using the sputtering tool at MESA+, this process is described in section 3.1.3. The degradation of the layer was still observed but starting with an un-switched piece of the sample enough scans could be made before the degradation starts.

7.4 Conclusions

The observation of the restructuring of the PZT(37/63) using an AFM was the main goal for this research. It is clearly seen that a reconfiguration of the domains takes place in a PZT(37/63) sample, unfortunately it is very hard to draw quantitative conclusions about the mechanisms behind it because the top-electrode does not seem to follow the underlying domain structure exactly. After several attempts to solve the problems using a metal top-electrode, it could not be solved within the given time.

It is clear that the domain structure in PZT(20/80) does not show the observed restructuring of the domain pattern. This observation is in agreement with the expectations based on the XRD measurements from chapter 4 and the calculations from the article by *Su et al.* [19].

Chapter 8

Conclusions

8.1 General conclusions

8.1.1 Mapping the domain dynamics

The main question that started this research was whether it would be possible to observe some kind of motion or restructuring of the domain walls in a PZT thin film grown on SRO buffered STO. Despite a number of setbacks and secondary questions that arose, it was possible to show that indeed a reorganization of the domain structure occurs upon ferroelectrically switching the thin film. The results from chapter 7 show that on some areas of the sample, the domains find a new configuration. Whether the sample switches between two states, or it finds a new configuration each time it is switched could not be concluded based on the performed measurements. Interesting to notice is the difference between a PZT(37/63) sample and a PZT(20/80) sample. Where the domains appear to reorganize in a PZT(37/63) sample, pinning of the domain structure is observed in a PZT(20/80) sample. This is similar to the observations done with X-ray analysis. This compositional difference can most likely be accounted to the difference in unit-cell parameters, the PZT(20/80) is more tetragonal meaning it has a longer axis in the length direction of the unit-cell compared to the PZT(37/63). The difference in tetragonality somehow increases the domain-wall switching energy, making them less likely to move. The pinning of a-domains in a PZT(20/80) can be assigned to a combination of the surrounding depolarization field and the stress field at the misfit dislocation-pairs [19].

Despite the fact that it was accomplished to observe a reorganization in the domain structure, it was not possible to do a qualitative analysis of this restructuring.

Issues with the top-electrode made it impossible to draw conclusions regarding for instance a- and c-domain fractions. Although the data from chapter 6 showed that the angling of the surface structure matches the expected angles based on the lattice parameters, the AFM is relatively not accurate enough to use it as an exact tool for measuring the domain angling, the XRD is a more accurate method of doing this. However, once one knows to some extend what the domain structure should be, the AFM turns out to be a useful tool to locally map the domain structure, something that is nog possible with an XRD because this technique maps observations to reciprocal space. Compared to PFM, the advantage of the AFM is that it is more stable and relatively easy to operate. Also PFM can not be used on a sample when there is a conducting top-electrode. On the other hand, the advantage of PFM is that also the different polarization directions of a- or c-domains can be mapped.

8.1.2 Thin top-electrode

At the start of this research, it was the question whether a very thin top-electrode on top of the PZT thin film would still allow one to map the underlying domain structure of the PZT using an AFM. It is shown that this is still the case for a metal top-electrode of about 10 nm. However, some difficulties arose from the fact that this top-electrode was not always able to follow the changes in the underlying domain structure. A crucial part in growing the metal top-electrode appeared to be a titanium adhesion layer, which significantly enhanced the attachment of the metal to the PZT thin film. Also the possibility of sputtering the top-electrode inside the cleanroom facility at the *MESA+* institute played a crucial part since it allowed the metal layer to be relatively free from particles.

8.2 Discussion and recommandations

8.2.1 Domain fractions

Throughout this thesis, different values for the c-domain fractions have been measured by different methods. These values do not seem to match which raises the question as to why this is. The different values are summarized in table 8.1.

The values in the table show quite some differences depending on the method of calculating them. In principle it is expected that the values for a PZT(37/63) and a PZT(40/60) sample do not differ that much from each other, because the

Method	$\phi_{c(20/80)}$	$\phi_{c(37/63)}{}^*$	$\phi_{c(37/63)}$	$\phi_{c(40/60)}$	Error	Comment
XRD	0.673	-	0.651	0.618	0.007	calc. from ω-χ-scans
XRD	0.699	-	0.681	0.609	0.02	calc. from lattice parm.
XRD	0.721	0.522	0.700	-	unknown	calc. from ω_{off}-values
TEM	0.707	-	-	-	0.04	Relative inaccurate
Theory	0.675	-	-	0.660	-	calc. from *K. Vergeer*

Table 8.1: Different values for the c-domain fractions calculated from different measurements. (*) This is for the PZT(37/63) after it was switched above the coercive field.

unit-cell sizes are pretty close to each other. Comparing the calculations based on the lattice parameters at different temperatures, it can be seen that they differ a lot for PZT(37/63) and PZT(40/60) which draws the measurement method into question.

The theoretical calculations done by *K. Vergeer* are based on adjustments to a model by *Pertsev* [21]. These calculations are done for the ideal case of epitaxial growth of PZT on SRO, and stress relaxation by domain forming. It is interesting to note that the values calculated from the ω-χ-scans, which are assumed to be fairly accurate, do match these calculations quite well.

The value that was measured from the TEM measurement raises by itself a lot of questions, because it is the question whether in this case the physical condition of the thin film is comparable to that of the other values. Most likely this is not the case because the sample is so thin that all the strain in one direction is completely gone.

The calculations done on the ω_{off}-values from the XRD map scans are quite noteworthy because this is the only case where a value is calculated for the PZT(37/63) sample after it has been switched. This value could in principle also be measured with an ω-χ-scan, which is probably interesting to do in case of a follow-up research. The other methods do not allow for a calculation of this value since the physical state of the sample changes during or before this. Maybe in the future the theoretical understanding is at a level where the theoretical model might predict a value for this, but for now that is not the case. Unfortunately the ω_{off}-values do not really match to values from other measurements, which raises questions about the precision of this method. Nevertheless, the difference between the switched and un-switched state is noted and might also be something to explore in possible future research.

8.2.2 Sub-domain patterns

One of the big questions arising from this research is the nature of the small sub-domain patterns that are observed and described in chapter 6. Quite some different measurement methods have been used to try to get an understanding of these patterns. Despite all the effort, the question still remains mainly unanswered. Since the phenomena occurs at all made samples of both compositions in this research, it is clear that this is more than a random artifact and therefore possibly contributes to the overall knowledge about the structure of tetragonal ferroelectric thin films.

If this subject would form a starting point for future research it is interesting to use a XRD with a very small X-ray bundle to be able to very locally measure the crystal structure. Also the use of a more precise AFM setup might give results leading to a better understanding of these patterns.

8.2.3 Top-electrode

The main challenge of this research appeared to be the top-electrode that should be used to switch the sample. The electrode should be conducting to be able to functions as an electrode, but also should be as thin as possible to be able to follow the the surface patterns of the PZT and should be flexible to follow the changes in the underlying surface patterns.

The use of a conducting perovskite oxide material as top-electrode would be an obvious choice because the material could be grown epitaxially on top of the PZT thin film during PLD process. The advantage of an epitaxial grown top-electrode would be that the electrode is expected to be able to follow the surface pattern changes while being attached to the PZT very strongly. Prior to this research a 100nm thick epitaxial grown SRO thin film was used as top-electrode in a lot of PZT samples, however looking at the surfaces of these samples the domain structure appears to be invisible. In this research a SRO thin film of 10nm thick was tried as top-electrode, but a more grain-like growth behavior was observed at the surface of these films instead of a smooth epitaxial thin film. Figure 8.1 shows an AFM scan of the surface of a 10nm SRO top-electrode film.

Despite the few attempts to grow a perovskite thin film as top-electrode in this research, for a potential follow-up on this work a further study on possible other perovskite materials or other thicknesses of SRO would be strongly recommended. During this research a thin metal layer seemed to be the way to go with in an early stage, so the idea of a perovskite top-electrode was given up. An important factor

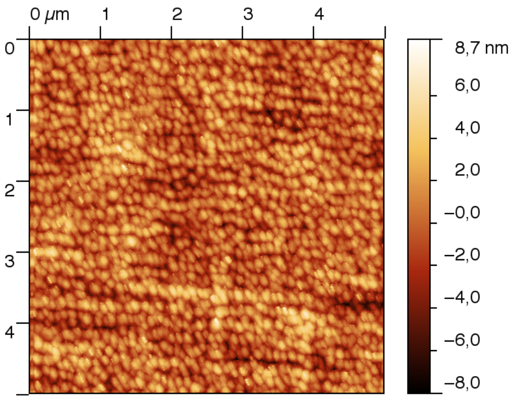

Figure 8.1: AFM scan of the surface of a PZT(20/80) sample with a 10nm SRO top-electrode thin film.

in this decision is the fact that the complete sample fabrication process is relatively time consuming. As described in chapter 3 a lot of process steps are needed to produce a finished sample, besides that the machines that were used are relatively popular and thus are booked quite a lot. The search for an epitaxial perovskite oxide top-electrode would probably require the production of a lot of new samples and therefore a lot of time.

8.2.4 Microlines

During this research the idea arose to use a relatively new lift-off fabrication technique, which is very suitable for PZT films, to produce a sample with very small micrometer lines [20]. The idea behind this is, at a certain width of the line the PZT thin film does not need to relax any stress in the direction perpendicular to the line. This would give a sample that consists only of domains oriented in one direction. The study on the movement or restructuring of these domains will possibly give new information about the fundamental mechanism that drives this motion.

The way the sample was fabricated is by depositing Aluminum-oxide on top of a single terminated STO substrate. After a relatively standard photo-lithography process, lines are etched away in the Aluminum-oxide. When then PZT is deposited using PLD, the PZT will grow epitaxial at the positions where the mask was removed and it will grow amorphous at the locations where there is still Aluminum-oxide. The amorphous PZT and Aluminum-oxide could be removed, but this requires a difficult chemical step which could also be ignored. The amorphous PZT is not expected to influence the epitaxial PZT next to it.

Unfortunately the fabricated sample did not show the expected behavior. This might be because the lines were simply too thick for the expected phenomena to occur, the smallest lines were 4μm. Another reason might be because there was still some clamping effect due to the material in between the PZT lines.

8.2.5 Domain movement in XRD analysis

The observations regarding the relaxation of the domain structure, as can be seen in Figures 4.1 and 4.3, were accidentally measured in a very late stadium of this research. It is because of this that this subject has not really been explored into further depth. Before this research started, the splitting of domain peaks in PZT(40/60) was observed in reciprocal map scans after switching the material above it's coercive field. During this research it was tested if the same would happen with PZT(37/63), which did. Because the changes in the reciprocal map scans also influenced the materials lattice parameters, it was tried to repeat the map scans making them more accurate. However, the sample that had been party switched before did no longer show the same orientations for the domain peaks. Because this discovery took place during the final stages of this research, it was decided to show the data but to put no extra effort in doing follow-up measurements.

Nevertheless the result is quite noteworthy because in some way the structure of the PZT thin film changes back to it's as-grown state, which probably influences the physical properties as well. It would be useful to combine the XRD data together with AFM measurements before and after relaxation because it can be expected that also there some changes to the structure might be observed. Also data about the piezoelectric behavior of the film would be useful to check if this influences the piezoelectric behavior.

Bibliography

[1] M. Nakajima, A. Wada, T. Yamada, Y. Ehara, T. Kobayashi, and H. Funakubo, *Impact of pulse poling on static and dynamic ferroelastic-domain contributions in tetragonal Pb(Ti, Zr)O_3 films determined by in-situ x?ray diffraction analysis* J. Appl. Phys. 116, 194102 (2014).

[2] Ruijuan Xu, Shi Liu, Ilya Grinberg, J. Karthik, Anoop R. Damodaran, Andrew M. Rappe and Lane W. Martin. *Ferroelectric polarization reversal via successive ferroelastic transitions*, Nature materials, 10.1038 (2014).

[3] Unpublished X-ray diffraction measurements performed by *K. Vergeer*. (2014)

[4] R.J.A. Steenwelle, PhD Thesis: *Strain and composition effects in epitaxial PZT thin films*, Chapter 2 and 4, (2012).

[5] C.M. Foster, W. Pompe, A.C. Daykin and J.S. Speck, *Relative coherency strain and phase transformation history in epitaxial ferroelectric thin films* J. Appl. Phys. 79-(3), (1996).

[6] H. Morioka, G. Asano, T. Oikawa, H. Funakubo, and K. Saito, *Large remanent polarization of 100% polar-axis-oriented epitaxial tetragonal* $Pb(Zr_{0.35}Ti_{0.65})O_3$ *thin films* J. Appl. Phys. 82, 4761 (2003).

[7] Y. Ehara, S. Utsugi, M. Nakajima, T. Yamada, T. Iijima, H. Taniguchi, M. Itoh, and H. Funakubo, *Spontaneous polarization estimation from the soft mode in strain-free epitaxial polar axis-oriented Pb(Zr,Ti)O_3 thick films with tetragonal symmetry* J. Appl. Phys. 98, 141914 (2011).

[8] J. E. Daniels, T. R. Finlayson, A. J. Studer, M. Hoffman, and J. L. Jones, *Time-resolved diffraction measurements of electric-field-induced strain in tetragonal lead zirconate titanate* J. Appl. Phys. 101, 094104 (2007).

[9] J.J. Broekmaat, PhD Thesis: *In-situ growth monitoring with scanning force microscopy during pulsed laser deposition* Chapter 3, (2008).

[10] B.F. Smith, PhD Thesis; *Ferroelectrics from the bottom up* Chapter 3, (2014).

[11] G. Catalan, A. Lubk, A.H.G. Vlooswijk, E. Snoeck, C. Magen, A. Janssens, G. Rispens, G. Rijders, D.H.A. Blank and B. Noheda, *Flexoelectric rotation of polarization in ferroelectric thin films* Nature materials, DOI:10.1038 (2011).

[12] C. Kittel, *Thickness of domain walls in ferroelectric and ferroelastic crystals* Sol. State. Comm., 10(1):119-121, (1972)

[13] J. Speck and W. Pompe, *Domain configurations due to multiple misfit relaxation machanisms in epitaxial ferroelectric thin films*, J. Appl. Phys., 76:466, (1994)

[14] M. Honig, J.A. Sulpizio, J. Drori, A. Joshua, E. Zeldov and S. Ilani, *Local electrostatic imaging of striped domain order in* $LaAlO_3/SrTiO_3$, Nature materials, DOI: 10.1038, (2013)

[15] F. Xu, S. Trolier-McKinstry, W. Ren and B. Xu, *Domain wall motion and its contribution to the dielectric and piezoelectric properties of lead zirconate titanate films* J. Appl. Phys, 89-(2), (2001)

[16] P. Chu, D. P. Chen, Y. L. Wang, Y. L. Xie, Z. B. Yan, J. G. Wan, J.-M. Liu and J. Y. Li, *[Kinetics of 90° domain wall motions and high frequency mesoscopic dielectric response in strained ferroelectrics: A phase-field simulation* Nature Scientific Reports, 4:5007, DOI:10.1038, (2014)

[17] V. Nagaragan, A. Roytburd, A Stanishevsky, S. Prasertchoung, T. Zhao, L. Chen, J. Melngailis, O. Auciello, R. Ramesh, *Dynamics of ferroelastic domains in ferroelectric thin films* Nature materials, DOI:10.1038, (2002)

[18] A. Vailionis, H. Boschker, W. Siemons, E. P. Houwman, D. H. A. Blank, G. Rijnders and G. Koster, *Misfit strain accommodation in epitaxial ABO3 perovskites: Lattice rotations and lattice modulations* Phys. Rev. B 83, 064101 (2011)

[19] D. Su, Q. Meng, C.A.F. Vaz, M-G Han, Y. Segal, F.J. Walker, M. Sawicki, C. Broadbridge, and C.H. Ahn, *Origin of 90° domain wall pinning in* $Pb(Zr_{0.2}Ti_{0.8})O_3$ *heteroepitaxial thin films*, App. Phys. Letters, 99, 102902, (2011)

[20] N. Banerjee, PhD Thesis; *Epitaxial perovskite oxide devices fabricated by lift-off technology*, Chapter 2, (2014)

[21] V. G. Kukhar, N. A. Pertsev, H. Kohlstedt, and R. Waser, *Polarization states of polydomain epitaxial* $Pb(Zr_{1-x}Ti_x)O_3$ *thin films and their dielectric properties*, Thys. Review B 73, 214103 (2006)